Journal of Ecology

The cost of resource use for photosynthesis drives variation in leaf nitrogen content across a climate and resource availability gradient

Journal:	*Journal of Ecology*
Manuscript ID	JEcol-2023-0933
Manuscript Type:	Research Article
Key-words:	ecophysiology, eco-evolutionary optimality, least-cost theory, leaf mass per area, leaf economics spectrum, plant functional ecology, photosynthesis, trait-gradient analysis

Abstract

1. Climate and resource availability are important determinants of plant nitrogen allocation. Photosynthetic least-cost theory provides a framework for understanding the integrative role of climate and soil resource availability on the nitrogen content of leaves, positing that water and nitrogen can be used as substitutable resources to support photosynthesis. The theory indicates that leaf investment in water use (reflected in the ratio of leaf intercellular to atmospheric CO_2, C_i:C_a) and nitrogen use (reflected in area-based leaf nitrogen content, N_{area}) are functions of the unit cost of using nitrogen relative to water (β) and aboveground climate, which alters demand for water and nitrogen to support photosynthesis. While promising, no study has tested this theory using concurrently measured β, leaf C_i:C_a, N_{area}, and components of N_{area} (leaf mass per area, M_{area}; mass-based leaf nitrogen content, N_{mass}).
2. We measured β, leaf C_i:C_a, N_{area}, M_{area}, and N_{mass} in 515 individuals comprising 57 species across 23 sites positioned along a precipitation and resource availability gradient in Texas, USA.
3. Leaf C_i:C_a was negatively related to N_{area}. This pattern was driven by negative relationships between leaf C_i:C_a and M_{area} coupled with no relationship between leaf C_i:C_a and N_{mass}, suggesting that nitrogen-water use tradeoffs expected from theory were driven by changes in leaf morphology. Increasing nitrogen availability was negatively associated with β, resulting in two pathways that contributed to positive effects of increasing nitrogen availability on N_{area}: (1) when mediated through negative effects of increasing nitrogen availability on β, positive relationships between β and leaf C_i:C_a, and negative relationships between leaf C_i:C_a and M_{area}, and (2) when mediated through negative effects of increasing nitrogen availability on β and negative relationships between β and N_{mass}. Increasing *VPD* increased N_{area} when mediated through negative effects of increasing *VPD* on leaf C_i:C_a and negative relationships between leaf C_i:C_a and M_{area}.
4. *Synthesis*. For the first time using concurrently measured β, leaf C_i:C_a, N_{area}, and components of N_{area}, we show that patterns expected from photosynthetic least-cost theory could explain much of the variance in leaf nitrogen content across a climatic and soil resource availability gradient.

Keywords: eco-evolutionary optimality, ecophysiology, least-cost theory, leaf mass per area, leaf economics spectrum, plant functional ecology, photosynthesis, trait-gradient analysis

Introduction

Terrestrial biosphere models, which comprise the land surface component of Earth system models, are sensitive to the formulation of photosynthetic processes (Knorr and Heimann 2001, Ziehn et al. 2011, Booth et al. 2012, Walker et al. 2021). This is because photosynthesis is the largest carbon flux between the atmosphere and terrestrial biosphere, and is constrained by ecosystem water and nitrogen cycles (Hungate et al. 2003, LeBauer and Treseder 2008, Fay et al. 2015, IPCC 2021). Many terrestrial biosphere models formulate photosynthesis by parameterizing photosynthetic capacity within plant functional groups through relationships between area-based leaf nitrogen content (N_{area}) and photosynthetic capacity (Kattge et al. 2009, Rogers 2014, Rogers et al. 2017). Models are beginning to include connected carbon-nitrogen cycles (Wieder et al. 2015, Shi et al. 2016, Davies-Barnard et al. 2020, Braghiere et al. 2022), which allows photosynthetic capacity to be predicted directly through N_{area} and indirectly through nitrogen availability (e.g., LPJ-GUESS, Smith et al. 2014, CLM5.0, Lawrence et al. 2019). Despite recent model developments, open questions remain regarding the generality of relationships between nitrogen availability and N_{area} across edaphic and climatic gradients.

Empirical support for positive relationships between nitrogen availability and N_{area} is abundant (Firn et al. 2019, Liang et al. 2020), and is a result attributed, in part, to the high nitrogen cost of building and maintaining Ribulose-1,5-bisphosphate carboxylase/oxygenase ("Rubisco"; Evans 1989a, Evans and Seemann 1989, Onoda et al. 2004, 2017, Walker et al. 2014, Dong et al. 2020). Such patterns imply that positive relationships between nitrogen availability and N_{area} increase photosynthetic capacity by increasing the maximum rate of Rubisco carboxylation. This integrated N_{area}-photosynthesis response to nitrogen availability has been observed both in manipulative experiments and across environmental gradients (Field and Mooney 1986, Evans 1989b, Walker et al. 2014, Li et al. 2020) and is thought to be driven by ecosystem nitrogen limitation, which limits primary productivity globally (LeBauer and Treseder 2008, Fay et al. 2015). However, this response is not consistently observed, as recent studies note variable N_{area}-photosynthesis relationships across differing levels of nitrogen availability (Liang et al. 2020, Luo et al. 2021, Waring et al. 2023) and that aboveground growing conditions (e.g.,

light availability, temperature, vapor pressure deficit) or species identity traits (e.g., photosynthetic pathway, nutrient acquisition strategy) may be more important for explaining variance in N_{area} and photosynthetic capacity across environmental gradients (Adams et al. 2016, Dong et al. 2017, 2020, 2022, Smith et al. 2019, Peng et al. 2021, Yan et al. 2023, Westerband et al. 2023).

One hypothesized mechanism to explain variance in N_{area} across environmental gradients has been proposed via photosynthetic least-cost theory. The theory posits that plants adapt and acclimate to their environment by optimizing photosynthetic assimilation rates at the lowest summed cost of nitrogen and water use (Wright et al. 2003). In a given environment, nitrogen and water use can be substituted for each other to maintain the lowest summed cost of resource use, such that optimal photosynthesis can be achieved with less efficient use of the more abundant and less costly resource to acquire in exchange for more efficient use of the less abundant and more costly resource to acquire. Photosynthetic least-cost theory predicts that, all else equal, an increase in nitrogen availability should decrease the cost of acquiring and using nitrogen relative to water for photosynthesis (a ratio referred to herein as β), resulting in optimal photosynthetic rates achieved with greater N_{area} at reduced stomatal conductance and ratio of leaf intercellular to atmospheric CO_2 (leaf C_i:C_a) (Wright et al. 2003, Prentice et al. 2014; Perkowski et al. *in review*). Alternatively, an increase in soil moisture should decrease costs of water acquisition and use for photosynthesis, increasing β, stomatal conductance, and leaf C_i:C_a, and resulting in optimal photosynthetic rates achieved with decreased N_{area} (Lavergne et al. 2020). The theory also predicts variability in stomatal conductance and N_{area} in response to climatic factors, suggesting that the optimal response to increased vapor pressure deficit (*VPD*) should be a reduction in stomatal conductance and leaf C_i:C_a that is counterbalanced by an increase in N_{area} to support the greater photosynthetic capacity needed to maintain photosynthetic rates at reduced conductance (Grossiord et al. 2020, López et al. 2021).

Variance in N_{area} across environmental gradients may depend on nutrient acquisition strategy, defined here as the method by which plants acquire nutrients (e.g., direct uptake, symbioses with soil microbial communities, etc.). For example, species that form associations with symbiotic nitrogen-fixing bacteria ("N-fixing species") should have access to less finite nitrogen supply than species not capable of forming such associations ("non-fixing species"), which may result in reduced β in N-fixing species. Decreased β could explain why N-fixing

species have greater leaf nitrogen content than non-fixing species (Adams et al. 2016, Dong et al. 2017), though these relationships have not been explored and may themselves be context dependent on external environmental factors such as nitrogen availability, temperature, or light availability (Taylor and Menge 2018, Friel and Friesen 2019, Perkowski et al. 2021, Waring et al. 2023).

Variance in N_{area} across environmental gradients may also depend on photosynthetic pathway. Generally, reduced leaf C_i:C_a in C_4 species suggests that C_4 species should have decreased β compared to C_3 species (Scott and Smith 2022), a pattern that could be the result of increased costs associated with water acquisition and use for photosynthesis, reduced costs of nitrogen acquisition and use for photosynthesis, or both. Theory predicts that decreased β values should allow C_4 species to have greater leaf nitrogen content compared to C_3 species, though opposite patterns are commonly observed, presumably due to increased nitrogen-use efficiency in C_4 species as a result of CO_2 concentrating mechanisms that constitute the C_4 photosynthetic pathway (Schmitt and Edwards 1981, Sage and Pearcy 1987, Ghannoum et al. 2011). No study has quantified β in C_4 species aside from the initial parameterization of β in a C_4 optimality model (Scott and Smith 2022).

While photosynthetic least-cost theory provides hypotheses for understanding integrated effects of climate and soil resource availability on N_{area}, empirical tests of the theory are limited. Despite growing evidence that supports patterns expected from the theory across environmental gradients (Paillassa et al. 2020, Querejeta et al. 2022, Westerband et al. 2023), studies have only explored theoretical expectations in C_3 species. Additionally, while N_{area} tends to covary with leaf C_i:C_a negatively across environmental gradients (Perkowski et al. *in review*, Dong et al. 2017, Paillassa et al. 2020, Westerband et al. 2023), no study has investigated effects of resource availability, nutrient acquisition strategy, or photosynthetic pathway using β as a predictor of variance in N_{area}. Finally, as N_{area} can be broken down into its component parts, leaf mass per area (M_{area}; g m^{-2}) and mass-based leaf nitrogen content (N_{mass}; gN g^{-1}), no study has investigated how the different components influence the hypothesized response of N_{area} to leaf C_i:C_a, which limits our ability to make inferences about whether variance in N_{area} across environmental gradients are driven by changes in leaf morphology (i.e., through changes in M_{area}), leaf chemistry (i.e., through changes in N_{mass}), or both.

Here, β, leaf C_i:C_a, N_{area}, N_{mass}, and M_{area} were measured in 515 individuals spanning 57 species across 23 grassland sites in Texas, USA. Texas contains a diverse climatic gradient, indicated by 2006-2020 mean annual precipitation across the 23 sites ranging from 563 to 1492 mm per year (Table 1; Fig. 2). Variability in nitrogen availability and soil moisture was expected across sites, owing to differences in soil texture and climate that would drive differential rates of water retention and nitrogen transformations to plant-available nitrogen substrate. We used the expected climatic and edaphic variability across sites to test the following hypotheses, outlined in Fig. 1:

1. Nitrogen availability will decrease β due to a reduction in costs of nitrogen acquisition, while soil moisture will increase β due to a reduction in costs of water acquisition. The ability to form symbiotic associations with N-fixing bacteria and presence of the C_4 photosynthetic pathway were each expected to decrease β.
2. Leaf C_i:C_a will be positively related to β, a pattern that will result in a negative indirect effect of increasing nitrogen availability on leaf C_i:C_a, a positive indirect effect of increasing soil moisture on leaf C_i:C_a, and decreased leaf C_i:C_a in both N-fixing species and C_4 species. Leaf C_i:C_a was expected to be negatively related to increasing *VPD*.
3. N_{area} will be negatively related to leaf C_i:C_a, which will be the result of either a negative relationship between N_{mass} and leaf C_i:C_a, a negative relationship between M_{area} and leaf C_i:C_a, or both. Negative covariance between components of N_{area} and leaf C_i:C_a will result in indirect positive and negative effects of increasing nitrogen availability and soil moisture, respectively, on N_{area}, and larger N_{area} in N-fixing species. C_4 species were expected to have decreased N_{area} compared to C_3 species due to greater nitrogen-use efficiency in C_4 species. Reductions in leaf C_i:C_a with increasing *VPD* were expected to increase N_{area}.

149 **Figure 1**

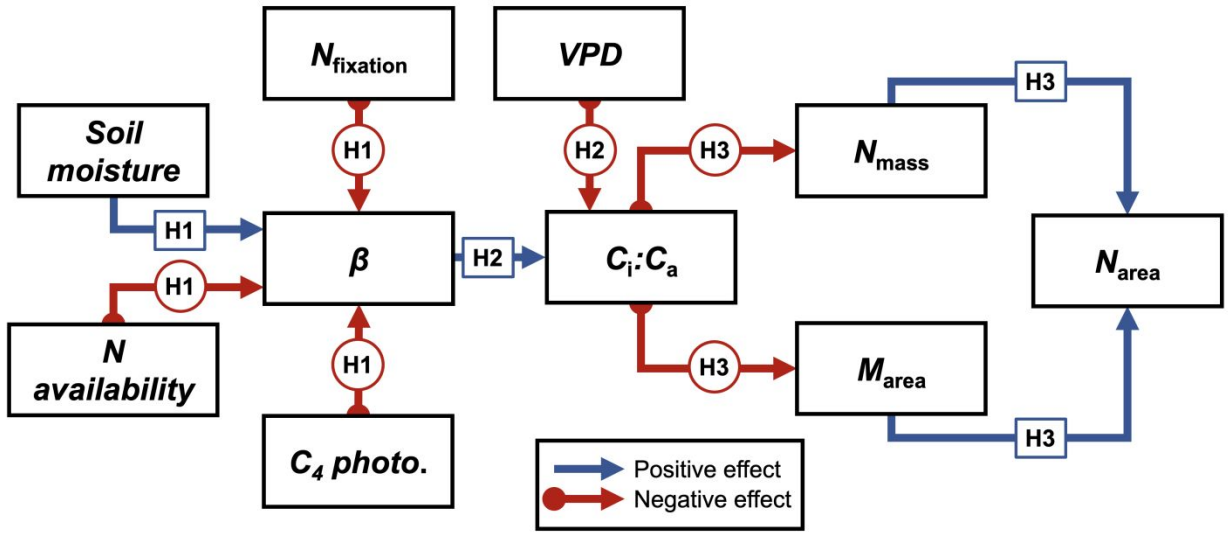

150

151 **Figure 1** Conceptual diagram mapping hypothesized paths that explain variance in area-based
152 leaf nitrogen content across environmental gradients. Hypothesized paths were generated
153 following expectations from photosynthetic least-cost theory (Wright et al. 2003, Prentice et al.
154 2014, Dong et al. 2017, 2020). Blue arrows indicate positive effects, while red arrows with
155 circular anchor points indicate negative effects. Red circular-anchored arrows indicate decreased
156 β in C_4 species compared to C_3 species and decreased β in N-fixing species compared to non-
157 fixing species. Indirect paths can be inferred by multiplying the sign of each arrow within the
158 designated path.

159

Methods

Site descriptions and sampling methodology

Leaf and soil samples were collected from 23 open canopy grassland sites across central and eastern Texas in summer 2020 and summer 2021 (Fig. 2). Eleven sites were visited between June and July 2020 and 15 sites (12 unique from 2020) were visited between May and June 2021. Sites were chosen to maximize precipitation and edaphic variability across sites (Table 1; Fig. 2). No site with personally communicated or anecdotal evidence of grazing or disturbance (e.g., mowing, feral hog activity, etc.) was used.

Leaf material was collected from three individuals of the five most abundant species at random locations across each site. All collected leaves were fully expanded with no visible herbivory or external damage and free from shading by nearby shrubs or trees. At least five soil samples were collected from 0-15cm below the soil surface at random locations in each site near the leaf collection sample locations. Soil samples were mixed by hand to create one composite soil sample per site.

Climate data

The Parameter-elevation Regressions on Independent Slopes Model ('PRISM', Daly et al. 2008) was used to access gridded daily temperature and precipitation estimates for the coterminous United States at a 4-km grid cell resolution between January 1, 2006 and July 31, 2021 (PRISM Climate Group, Oregon State University, https://prism.oregonstate.edu, data created 4 Feb 2014, accessed 24 Mar 2022). Daily air temperature, *VPD*, and precipitation data were extracted from the grid cell that contained the latitude and longitude of each property using the 'extract' function in the 'terra' R package (Hijmans 2022). PRISM data were used in lieu of local weather station data because several rural sites did not have a local weather station within a 20-km radius of the site. Total precipitation and mean *VPD* were calculated for the prior 1, 2, 3, 4, 5, 6, 7, 8, 9, 10, 15, 20, 25, 30, 60, and 90 days leading up to each site visit. Temperature data were not included in analyses due to the close range in mean annual temperature between sites (mean±SD: 19.8±0.9ºC; Table 1).

189 **Table 1** Site locality information, sampling year(s), 2006-2020 mean annual precipitation, 2006-
190 2020 mean annual temperature, and water holding capacity*

Site	Latitude	Longitude	Year	MAP	MAT	WHC
Edwards_2019_17	29.95	-100.36	2020	563.5	19.0	224.7
Uvalde_2020_02	29.59	-100.09	2020, 2021	648.5	19.5	235.2
Menard_2020_01	30.91	-99.57	2020	641.9	18.3	220.2
Kerr_2020_03	30.06	-99.34	2021	672.4	18.3	237.5
Bandera_2020_03	29.85	-99.30	2021	789.4	18.8	235.1
Sansaba_2020_01	31.29	-98.62	2020	733.0	18.8	234.3
Comal_2020_21	29.79	-98.43	2020	878.5	19.9	220.7
Blanco_2019_16	29.99	-98.43	2020	833.0	19.2	222.2
Bexar_2019_13	29.24	-98.43	2020	759.3	21.5	206.0
Burnet_2020_14	30.84	-98.34	2021	763.3	19.5	217.8
Comal_2020_19	30.01	-98.32	2021	845.0	19.3	220.4
Hays_2021_54	29.96	-98.17	2021	861.3	20.0	225.6
Burnet_2020_12	30.82	-98.06	2021	815.1	19.4	245.3
Williamson_2019_09	30.71	-97.86	2020	867.7	19.7	270.2
Williamson_2019_10	30.54	-97.77	2020	819.5	19.9	239.8
Bell_2021_08	31.06	-97.55	2021	937.3	19.6	232.3
Fayette_2021_12	29.86	-97.21	2021	985.7	20.4	165.6
Fayette_2020_09	29.86	-96.71	2021	1002.7	20.8	187.6
Washington_2020_08	30.28	-96.41	2021	1077.4	20.4	203.9
Austin_2020_03	29.78	-96.24	2021	1108.7	20.6	253.0
Brazos_2020_16	30.93	-96.23	2021	1078.0	20.1	202.2
Brazos_2020_18	30.52	-96.21	2020, 2021	1099.4	20.4	233.5
Harris_2020_03	29.88	-95.31	2020, 2021	1492.0	21.6	265.6

191

192 *Rows are arranged by longitude to visualize precipitation variability. Climate data were
193 calculated using monthly PRISM data between 2006 and 2020 from the 4-km grid cell that
194 contained each site. Key: MAP=2006-2020 mean annual precipitation (mm yr^{-1}); MAT=2006-
195 2020 mean annual temperature (°C); WHC=water holding capacity (mm)

196 **Figure 2**

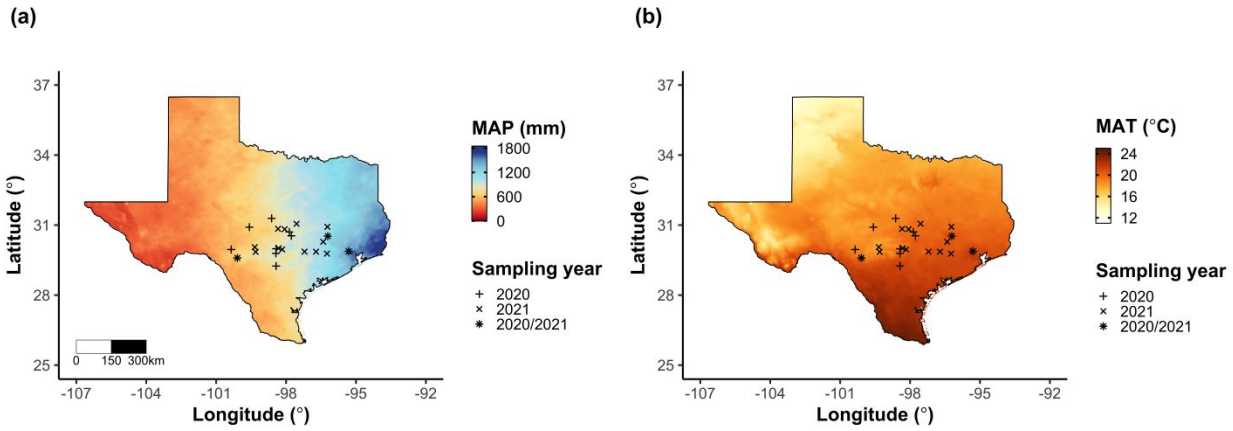

197

198 **Figure 2** Site locations along 2006-2020 mean annual precipitation (a) and mean annual
199 temperature (b) gradients in Texas, USA. Precipitation and temperature data were plotted at a 4-
200 km grid resolution using monthly PRISM data between 2006 and 2020. In both panels, addition
201 signs ("+") refer to sites visited in 2020, multiplication signs ("x") to sites visited in 2021, and
202 asterisks ("*") to sites visited in both 2020 and 2021. The distance scale bar in (a) applies to (b).

203

Edaphic characteristics

Composited soil samples were sent to the Texas A&M Soil, Water and Forage Laboratory to quantify soil nitrate concentration (NO_3-N; ppm), which was used as a proxy for nitrogen availability. Soil NO_3-N was determined by extracting composite soil samples in 1 M KCl, measuring absorbance of extracts at 520 nm using the end product of a NO_3-N to NO_2-N cadmium reduction reaction (Keeney and Nelson 1983, Kachurina et al. 2000). Soil texture data (% sand, % silt, % clay) were estimated on a volume basis using the simple jar method and a graduated cylinder.

Soil moisture was estimated using the 'Simple Process-Led Algorithms for Simulating Habitats' model ('SPLASH'; Davis et al. 2017). This model, derived from the STASH model (Cramer and Prentice 1988), spins up a bucket model using Priestley-Taylor equations (Priestley and Taylor 1972) to calculate daily soil moisture (W_n; mm) as a function of the previous day's soil moisture (W_{n-1}; mm), daily precipitation (P_n; mm), condensation (C_n; mm), actual evapotranspiration (E_n^a; mm), and runoff (RO; mm):

$$W_n = W_{n-1} + P_n + C_n - E_n^a - RO \quad (1)$$

Models were spun up by equilibrating the previous day's soil moisture using successive model iterations with daily mean air temperature, daily precipitation total, the number of daily sunlight hours, and latitude as model inputs (Davis et al. 2017). Daily sunlight hours were estimated for each day at each site using the 'getSunlightTimes' function in the 'suncalc' package in R, which estimated sunrise and sunset times of each property using date and site coordinates (Thieurmel and Elmarhraoui 2019). Water holding capacity (mm), or bucket size, was estimated as a function of soil texture using pedotransfer equations explained in Saxton and Rawls (2006), as done in Stocker et al. (2020) and Bloomfield et al. (2022). A summary of these equations is included in the *Supplemental Information*.

Daily soil moisture outputs for each site were used to calculate mean daily soil moisture for the prior 1, 2, 3, 4, 5, 6, 7, 8, 9, 10, 15, 20, 25, 30, 60, and 90 days leading up to each site visit. All soil moisture estimates were then expressed as a fraction of water holding capacity to normalize values across sites as done in Stocker et al. (2018).

Leaf trait measurements

Images of each leaf were taken following each site visit using a flat-bed scanner. Fresh leaf area was determined from each image using the 'LeafArea' R package (Katabuchi 2015), which automates leaf area calculations using ImageJ software (Schneider et al. 2012). Each leaf was dried at 65°C for at least 48 hours to a constant mass, weighed, and manually ground with a mortar and pestle until homogenized. Leaf mass per area (M_{area}; g m^{-2}) was calculated as the ratio of dry leaf biomass to fresh leaf area. Subsamples of dried and homogenized leaf tissue were used to measure mass-based leaf nitrogen content (N_{mass}; gN g^{-1}) through elemental combustion analysis (Costech-4010, Costech Instruments, Valencia, CA). Area-based leaf nitrogen content (N_{area}; gN m^{-2}) was calculated as the product of N_{mass} and M_{area}.

Subsamples of dried and homogenized leaf tissue were sent to the University of California-Davis Stable Isotope Facility to determine leaf $\delta^{13}C$ (‰; relative to Vienna Pee Dee Belemnite international reference standard). Leaf $\delta^{13}C$ was measured using an elemental analyzer (PDZ Europa ANCA-GSL; Sercon Ltd., Chestshire, UK) interfaced to an isotope ratio mass spectrometer (PDZ Europa 20-20 Isotope Ratio Mass Spectrometer, Sercon Ltd., Chestshire, UK). Leaf $\delta^{13}C$ was used to estimate the ratio of intercellular (C_i) to extracellular (C_a) CO_2 ratio (leaf C_i:C_a; unitless) following the approach explained in Farquhar et al. (1989):

$$Leaf\ \frac{C_i}{C_a} = \frac{\Delta^{13}C - a}{b - a} \quad (2)$$

where a represents the fractionation between ^{12}C and ^{13}C due to diffusion in air, assumed to be 4.4‰, and b represents the fractionation caused by Rubisco carboxylation, assumed to be 27‰ (Farquhar et al. 1989). $\Delta^{13}C$ represents the relative difference between leaf $\delta^{13}C$ (‰) and $\delta^{13}C$ in air (assumed to be -8‰; Farquhar et al. 1989), and is calculated as:

$$\Delta^{13}C = \frac{\delta^{13}C_{air} - \delta^{13}C_{leaf}}{1 + \delta^{13}C_{leaf}} \quad (3)$$

For C_4 species, b in Eqn. 1 was set to 6.3‰, derived from:

$$b = c + (d\varphi) \quad (4)$$

Where c was assumed as -5.7‰ and d was assumed as 30‰ (Farquhar et al. 1989). φ is the bundle sheath leakiness term and was assumed as 0.4. All leaf C_i:C_a values less than 0.1 and greater than 0.95 were assumed to be incorrect and removed from the analysis, resulting in the removal of 24 data points (<5% of dataset).

The cost of acquiring and using nitrogen relative to water for photosynthesis (β) was derived using leaf C_i:C_a and site climate data using equations described in Prentice et al. (2014) and Lavergne et al. (2020):

$$\beta = 1.6\eta^* VPD \frac{\left(\chi - \frac{\Gamma^*}{C_a}\right)^2}{(1-\chi)^2 \cdot (K + \Gamma^*)} \quad (5)$$

where η^* is the viscosity of water relative to its viscosity at 25ºC, calculated using mean air temperature of the seven days leading up to each site visit following equations in Huber et al. (2009). *VPD* (Pa) was set to the mean of the seven days leading up to each site visit, while C_a represents atmospheric CO_2 concentration, approximated as 420 μmol mol^{-1} CO_2. Atmospheric CO_2 concentration was converted to partial pressure (Pa) and corrected for elevation using the product of an elevation correction for atmospheric pressure described in Stocker et al. (2020):

$$P_{atm,z} = P_{atm,0}\left(1 - \frac{Lz}{T_{K,0}}\right)^{gM_a(RL)^{-1}} \quad (6)$$

where $P_{atm,z}$ (Pa) is atmospheric pressure at elevation z (m.a.s.l.), $P_{atm,0}$ is atmospheric pressure at 0 m.a.s.l. (101325 Pa), L is the mean adiabatic lapse rate (0.0065 K m^{-2}), $T_{K,0}$ is temperature in K at 25ºC (298.15 K), g is the gravitational acceleration rate (9.80665 m s^{-2}), M_a is the molar weight of dry air (0.028963 kg mol^{-1}), and R is the universal gas constant (8.3145 J mol^{-1}).

In Eqn. 5, K (Pa) is the Michaelis-Menten coefficient for Rubisco affinity to CO_2 and O_2, calculated as:

$$K = K_c\left(1 + \frac{O_i}{K_o}\right) \quad (7)$$

where K_c (Pa) and K_o (Pa) are the Michaelis-Menten coefficients for Rubisco affinity to CO_2 and O_2, respectively. O_i is the intercellular O_2 concentration, set to 210 μmol mol^{-1} and converted to partial pressure (Pa) using the elevation correction explained in Eqn. 6. In Eqn. 5, Γ^* (Pa) is the CO_2 compensation point in the absence of dark respiration. K_c, K_o, and Γ^* were each calculated following Bernacchi et al. (2001), where:

$$K_c = 404.9 * exp^{\left(\frac{79430(T_k - 298)}{298RT_k}\right)} \quad (8a)$$

$$K_o = 278.4 * exp^{\left(\frac{36380(T_k - 298)}{298RT_k}\right)} \quad (8b)$$

$$\Gamma^* = 42.75 * exp^{\left(\frac{37830(T_k - 298)}{298RT_k}\right)} \quad (8c)$$

In all three equations, T_k is leaf temperature (in Kelvin), estimated through mean daily air temperature of the seven days leading up to each site visit, while R is the universal gas constant (8.314 J mol^{-1} K^{-1}). K_c, K_o, and Γ^* were each converted to partial pressure using the elevation correction equation explained in Eqn. 6.

Plant functional groups

Plant functional group was assigned to each species and used as the primary descriptor of species identity. Functional groups were assigned based on photosynthetic pathway (C_3, C_4) and ability to form associations with symbiotic N-fixing bacteria (N-fixer, non-fixer). The ability to form associations with symbiotic N-fixing bacteria was assigned based on whether species were in the *Fabaceae* family, as no other families known to include N-fixing species were collected. Photosynthetic pathway of each species was determined from past literature and confirmed through leaf $\delta^{13}C$, and no collected plant used the CAM photosynthetic pathway. Functional groups were chosen based on *a priori* hypotheses regarding the functional role of nitrogen fixation and photosynthetic pathway on the sensitivity of plant nitrogen uptake to nitrogen availability and aboveground growing conditions. Functional group classifications resulted in three distinct groups within the dataset: C_3 N-fixers (n=52 individuals comprising 5 species), C_3 non-fixers (n=346 individuals comprising 41 species), and C_4 non-fixers (n=117 individuals comprising 11 species).

Data analysis

Analyses and plots were conducted in R version 4.1.1 (R Core Team 2021). A series of separate linear mixed effects models were constructed to investigate drivers of β, leaf C_i:C_a, N_{area}, N_{mass}, and M_{area}, followed by a path analysis to examine direct and indirect drivers of variance in N_{area}.

To address our first hypothesis and investigate primary drivers of β, we constructed a linear mixed effects model where β was regressed against soil moisture, nitrogen availability, and functional group, in addition to all possible interactions between soil moisture, nitrogen availability, and functional group. β was square root transformed to normalize model residuals, and species was designated as a random intercept term. An information-theoretic model selection approach was used to determine whether 90-, 60-, 30-, 20-, 15-, 10-, 9-, 8-, 7-, 6-, 5-, 4-, 3-, 2-, or 1-day mean daily soil moisture conferred the best model fit. To do this, 16 separate linear

mixed effect models were constructed where square root transformed β was included as the response variable and each soil moisture timestep was separately included as a single continuous fixed effect. Species were included as a random intercept term for all models. Corrected Akaike Information Criterion (AICc) and root mean square error (RMSE) values were used to select the soil moisture timescale that conferred the best model fit, indicated by the model with the lowest AICc and RMSE (Table S2; Fig. S1).

To address our second hypothesis and explore primary drivers of leaf C_i:C_a, a second linear mixed effect model regressed leaf C_i:C_a against *VPD*, soil moisture, nitrogen availability, and functional group, in addition to interactions between *VPD* and functional group and all possible interactions between soil moisture, nitrogen availability, and functional group as done for the β model explained above. Species were included as a random intercept term. We used an information-theoretic model selection approach to determine whether 90-, 60-, 30-, 20-, 15-, 10-, 9-, 8-, 7-, 6-, 5-, 4-, 3-, 2-, or 1-day mean daily *VPD* conferred the best model fit for leaf C_i:C_a following the same approach explained above for the soil moisture effect on β. Soil moisture was set to the same timescale that conferred the best fit for the β model explained above.

Finally, to address our third hypothesis and investigate drivers of N_{area} as well as components of N_{area} (N_{mass} and M_{area}), a third set of linear mixed effects models was constructed for each of N_{area}, N_{mass}, and M_{area}. Each model regressed either N_{area}, N_{mass}, or M_{area} against leaf C_i:C_a, soil moisture, nitrogen availability, and functional group, in addition to an interaction between leaf C_i:C_a and functional group and all possible interactions between soil moisture, nitrogen availability, and functional group as done for the β model explained above. Species were included in all models as a random intercept term. All response variables (N_{area}, N_{mass}, and M_{area}) were log-transformed to normalize model residuals. Soil moisture was set to the same timescale that conferred the best fit for β as explained above.

In all linear mixed-effect models explained above, including those used to select relevant timescales, we used the 'lmer' function in the 'lme4' R package (Bates et al. 2015) to fit each model and the 'Anova' function in the 'car' R package (Fox and Weisberg 2019) to calculate Type II Wald's χ^2 and determine the significance level (α=0.05) of each fixed effect coefficient. We also used the 'emmeans' R package (Lenth 2019) to conduct post-hoc comparisons using Tukey's tests, where degrees of freedom were approximated using the Kenward-Roger approach (Kenward and Roger 1997).

Finally, a path analysis was constructed using a piecewise structural equation model to examine direct and indirect pathways that contributed to variance in components of N_{area} across the environmental gradient. The structural equation model included all patterns expected from photosynthetic least-cost theory (outlined in Fig. 1), and any additional pathway for which we could generate an *a priori* hypothesis. Specifically, additional paths were added to investigate the following hypothesized direct effects: positive effects of increasing nitrogen availability on N_{mass} and M_{area} (Poorter et al. 2009, Firn et al. 2019, Liang et al. 2020), reduced leaf C_i:C_a, N_{mass}, and M_{area} in C_4 species compared to C_3 species (Schmitt and Edwards 1981, Sage and Pearcy 1987, Poorter et al. 2009, Ghannoum et al. 2011), greater N_{mass} in N-fixing species compared to non-fixing species (Adams et al. 2016, Dong et al. 2017, Bytnerowicz et al. 2023), negative effects of increasing β on N_{mass} (expected from theory if variance in N_{mass} is independent of leaf C_i:C_a), negative covariance between M_{area} and N_{mass} (Onoda et al. 2004, 2017), positive covariance between soil moisture and nitrogen availability (Reynolds et al. 2007), and negative covariance between *VPD* and soil moisture (Brzostek et al. 2014).

Given hypotheses explained above, seven separate linear mixed effect models were loaded into the structural equation model: (1) log-transformed N_{area} regressed against log-transformed N_{mass} and log-transformed M_{area}, (2) log-transformed M_{area} regressed against leaf C_i:C_a, nitrogen availability, and photosynthetic pathway, (3) log-transformed N_{mass} regressed against leaf C_i:C_a, square-root transformed β, nitrogen availability, log-transformed M_{area}, N-fixation ability, and photosynthetic pathway, (4) leaf C_i:C_a regressed against square-root transformed β, *VPD*, photosynthetic pathway, and soil moisture, (5) square-root transformed β regressed against nitrogen availability, soil moisture, N-fixation ability, and photosynthetic pathway, and *VPD*, (6) nitrogen availability regressed against soil moisture, and (7) soil moisture regressed against *VPD*. All models included the relevant timescale selected in the individual linear mixed-effect models explained above and included species as a random intercept term. Models were built using the 'lme' function in the 'nlme' R package (Pinheiro and Bates 2022), and were loaded into the piecewise structural equation model using the 'psem' function in the 'piecewiseSEM' R package (Lefcheck 2016).

Tests of directed separation indicated that the structural equation model was missing three correlations that contributed to poor overall model fit (Fisher's C=162.814, p<0.001; df=42; AIC=246.814; BIC=418.649): a correlation between nitrogen availability and VPD_{90}

(p<0.001), a correlation between β and *VPD* (p<0.05), and a correlation between soil moisture and N_{mass} (p<0.05). These relationships were included in the model as correlated errors, as we did not have hypotheses to explain their direct relationships. The inclusion of these relationships as correlated errors improved model fit (Fisher's C=23.899, p=0.939; df=36; AIC=107.899; BIC=279.734) and satisfied goodness-of-fit recommendations for piecewise structural equation models (Lefcheck 2016).

Results

Cost to acquire nitrogen relative to water (β)

Model selection indicated that 90-day soil moisture conferred the best model fit for β (AICc=3058.9; Table S2; Fig. S1). Increasing nitrogen availability decreased β (p=0.001; Table 2; Fig. 3a) similarly between functional groups (nitrogen-by-functional group interaction: p>0.05; Table 2). An interaction between soil moisture and functional group (p=0.001; Table 2) indicated that positive effects of increasing soil moisture on β (p<0.05; Table 2; Fig. 3b) were driven by C_3 non-fixers (Tukey test of the soil moisture-β slope: p<0.001; Fig. 3b), as there was no effect of soil moisture on β in C_3 N-fixers or C_4 non-fixers (Tukey test of the soil moisture-β slope: p>0.05 in both functional groups). A functional group effect (p<0.001; Table 2) indicated that C_4 non-fixers had reduced β compared to C_3 N-fixers and C_3 non-fixers (Tukey: p<0.001 in both cases), while β did not differ between C_3 N-fixers and C_3 non-fixers (Tukey: p>0.05).

Table 2 Effects of soil moisture, nitrogen availability, and plant functional group on the cost to acquire nitrogen relative to water*

	df	Coefficient	χ^2	*p*
Intercept	-	$1.96*10^{1}$	-	-
Soil moisture (SM_{90})	1	$5.80*10^{0}$	7.982	**0.004**
N availability (N)	1	$-3.20*10^{-1}$	10.461	**0.001**
PFT	2	-	98.254	**<0.001**
SM_{90} * N	1	$7.45*10^{-1}$	0.741	0.389
SM_{90} * PFT	2	-	13.922	**0.001**
N * PFT	2	-	1.588	0.452
SM_{90} * N * PFT	2	-	1.061	0.588

*Significance determined using Type II Wald χ^2 tests (α=0.05). *p*-values less than 0.05 are in bold. Model coefficients are expressed on the square root scale and are only included for continuous fixed effects. Key: df=degrees of freedom, χ^2=Wald Type II chi-square test statistic; β=unit cost of acquiring and using nitrogen relative to water

410 **Figure 3**

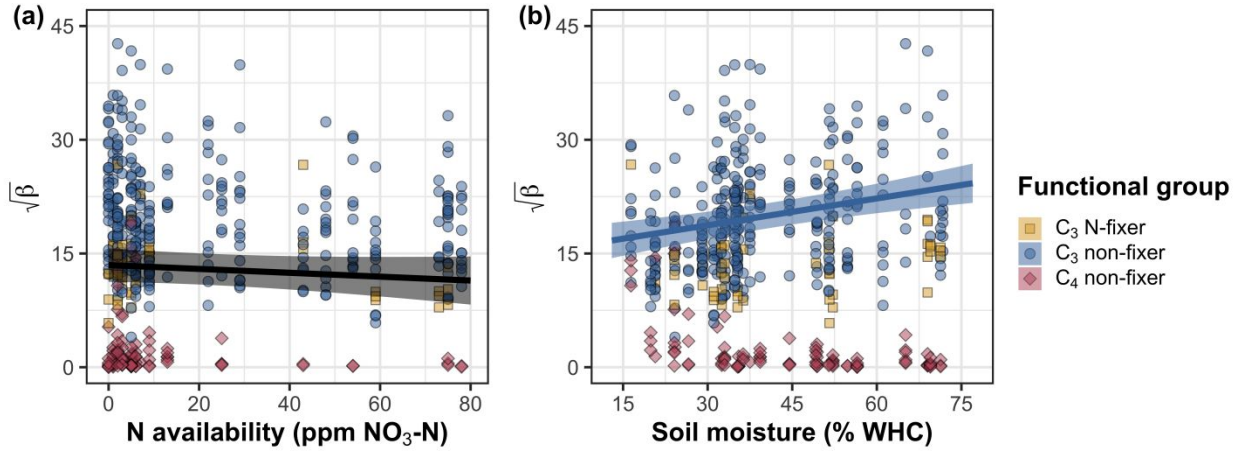

411

412 **Figure 3** Effects of nitrogen availability (a) and soil moisture (b) on the cost of acquiring
413 nitrogen relative to water (β). β is included on the y-axis for both panels as square root
414 transformed values to normalize model residuals. Yellow square-shaped points represent C_3 N-
415 fixers, blue circular-shaped points represent C_3 non-fixers, and red diamond-shaped points
416 represent C_4 non-fixers. Black trendlines and 95% confidence intervals demonstrate significant
417 relationships (p<0.05) averaged across functional groups, only drawn when there was no
418 interaction between functional group and the independent variable on the x-axis. Colored
419 trendlines and 95% confidence intervals indicate significant relationships (p<0.05) within
420 functional groups, only drawn when there was an interaction between functional group and the
421 independent variable on the x-axis. Trendlines are drawn using model predictions using the
422 'emmeans' R package (Lenth 2019) across the range in x-axis values.

423

Leaf C_i:C_a

Model selection indicated that 90-day mean *VPD* (VPD_{90}) conferred the best model fit for leaf C_i:C_a (AICc=-906.72; Table S2; Fig. S1). Increasing VPD_{90} decreased leaf C_i:C_a (p<0.001; Table 3; Fig. 4a) similarly across functional groups (VPD_{90}-by-functional group interaction: p>0.05; Table 3). An interaction between soil moisture and functional group (p<0.001; Table 3) indicated that negative effects of increasing soil moisture on leaf C_i:C_a (p<0.05; Table 3) were driven by C_4 non-fixers (Tukey test of the soil moisture-leaf C_i:C_a slope: p<0.001; Fig. 4b), as there was no effect of soil moisture on leaf C_i:C_a in C_3 N-fixers or C_3 non-fixers (Tukey test of the soil moisture-leaf C_i:C_a slope: p>0.05 for both functional groups). An interaction between nitrogen availability and functional group (p<0.001; Table 3) revealed that negative effects of increasing nitrogen availability on leaf C_i:C_a (p<0.05; Table 3) were driven by C_4 non-fixers (Tukey: p<0.001; Fig. 4c), as there was no effect of nitrogen availability on leaf C_i:C_a in C_3 N-fixers or C_3 non-fixers (Tukey test of the soil moisture-leaf C_i:C_a slope: p>0.05 in both functional groups). Finally, a functional group effect (p<0.001; Table 3) indicated that C_4 non-fixers had reduced leaf C_i:C_a compared to C_3 N-fixers and C_3 non-fixers (Tukey: p<0.001 in both cases), while leaf C_i:C_a did not differ between C_3 N-fixers and C_3 non-fixers (Tukey: p>0.05).

441 **Table 3** Effects of *VPD*, drivers of the cost to acquire nitrogen relative to water, and functional
442 group on leaf C_i:C_a*

Treatment	df	Coefficient	χ^2	*p*
Intercept	-	$1.15*10^{0}$	-	-
Vapor pressure deficit (VPD_{90})	1	$-2.89*10^{-1}$	20.775	**<0.001**
Soil moisture (SM_{90})	1	$-1.03*10^{-1}$	7.711	**0.005**
N availability (N)	1	$-3.26*10^{-3}$	6.359	**0.012**
PFT	2	-	721.308	**<0.001**
SM_{90} * N	1	$8.18*10^{-3}$	0.091	0.763
VPD_{90} * PFT	2	-	3.675	0.159
SM_{90} * PFT	2	-	17.509	**<0.001**
N * PFT	2	-	22.486	**<0.001**
SM_{90} * N * PFT	2	-	1.826	0.401

443

444 *Significance determined using Type II Wald χ^2 tests (α=0.05). *P*-values less than 0.05 are in
445 bold. Leaf C_i:C_a was not transformed prior to model fitting, so model coefficients are reported on
446 the response scale. Model coefficients are only included for continuous fixed effects and are
447 reported on the response scale. Key: df=degrees of freedom, χ^2=Wald Type II chi-square test
448 statistic
449

Figure 4

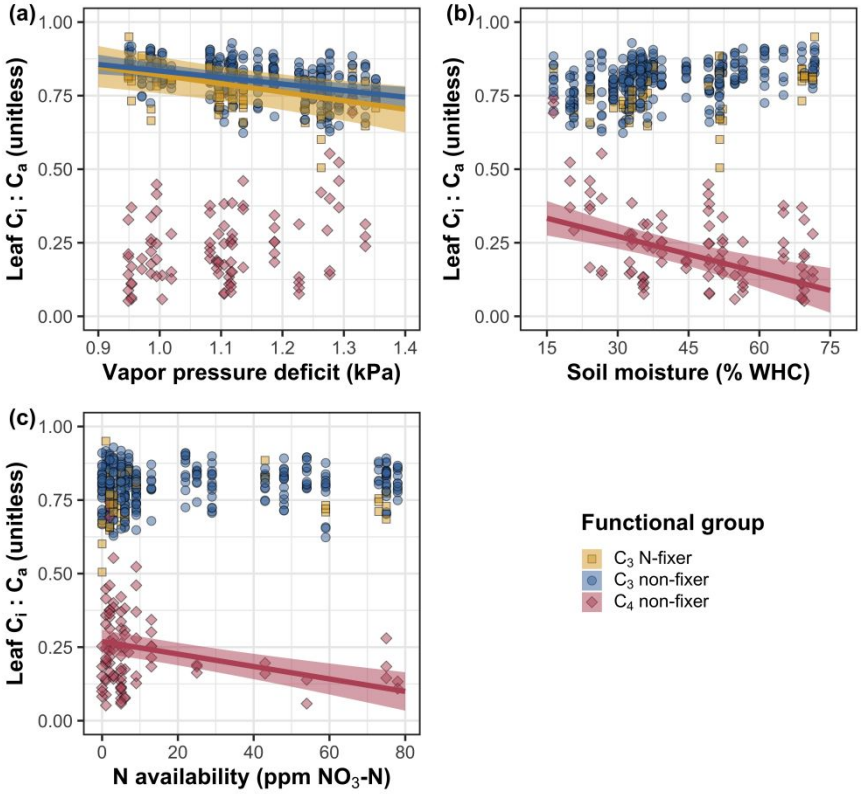

Figure 4 Effects of vapor pressure deficit (a), soil moisture (b), and nitrogen availability (c) on leaf C_i:C_a. Colors and shapes are as explained in Figure 3. Colored trendlines and 95% confidence intervals demonstrate significant relationships (p<0.05) within functional groups. Trendlines are drawn using model predictions using the 'emmeans' R package (Lenth 2019) across the range in x-axis values.

458 *Leaf nitrogen content*

459 An interaction between leaf C_i:C_a and functional group (p<0.001; Table 4) revealed that negative
460 effects of increasing leaf C_i:C_a on N_{area} (p<0.05; Table 4) were driven by C_3 non-fixers and C_3 N-
461 fixers (Tukey test of the leaf C_i:C_a-N_{area} slope: p<0.05 for both functional groups; Fig. 5a), as
462 there was no leaf C_i:C_a-N_{area} relationship in C_4 non-fixers (Tukey test of the leaf C_i:C_a-N_{area} slope
463 in C_4 non-fixers: p>0.05). Increasing nitrogen availability and soil moisture each increased N_{area}
464 (p<0.05 in both cases; Table 4; Fig. 5b-c) similarly between functional groups (nitrogen-by-
465 functional group interaction and soil moisture-by functional group interaction: p>0.05; Table 4).
466 A functional group effect (p<0.001; Table 4) indicated that C_4 non-fixers had reduced N_{area}
467 compared to C_3 N-fixers and C_3 non-fixers (Tukey: p<0.05 in both cases), while C_3 N-fixers had
468 slightly greater N_{area} than C_3 non-fixers (Tukey: p<0.1).

469 There was no relationship between leaf C_i:C_a and N_{mass} (p>0.05; Table 4; Fig. 5d). A
470 weak interaction between nitrogen availability and soil moisture (p<0.05; Table 4) indicated that
471 the positive effect of increasing nitrogen availability on N_{mass} (p<0.001; Table 4; Fig. 5e)
472 decreased with increasing soil moisture despite a positive effect of increasing soil moisture on
473 N_{mass} (p<0.05; Table 4; Fig. 5f). A functional group effect (p<0.001; Table 4) indicated that C_4
474 non-fixers had slightly reduced N_{mass} compared to C_3 N-fixers (Tukey: p<0.1), but N_{mass} in C_4
475 non-fixers did not differ from C_3 non-fixers (Tukey: p>0.05), nor did N_{mass} differ between C_3 N-
476 fixers and C_3 non-fixers (Tukey: p>0.05).

477 An interaction between leaf C_i:C_a and functional group (p<0.001; Table 4) revealed that
478 negative effects of increasing leaf C_i:C_a on M_{area} (p<0.05; Table 4) were driven by C_3 N-fixers
479 and C_3 non-fixers (Tukey test of the leaf C_i:C_a-M_{area} slope: p<0.001 for both functional groups;
480 Fig. 5g), as there was no leaf C_i:C_a-M_{area} relationship in C_4 non-fixers (Tukey test of the leaf
481 C_i:C_a-M_{area} slope: p>0.05). A three-way interaction between nitrogen availability, soil moisture,
482 and functional group (p<0.05; Table 4) indicated that negative effects of increasing nitrogen
483 availability on M_{area} in C_3 non-fixers (Tukey test of the nitrogen-M_{area} slope in C_3 non-fixers:
484 p<0.001; Fig. 5h) became increasingly negative with increasing soil moisture, while positive
485 effects of increasing nitrogen availability on M_{area} in C_3 N-fixers (Tukey test of the nitrogen-M_{area}
486 slope in C_3 N-fixers: p<0.05; Fig. 5h) increased with increasing soil moisture. There was no
487 effect of nitrogen availability on M_{area} in C_4 non-fixers regardless of soil moisture threshold.
488 There was also no individual effect of soil moisture on M_{area} (p>0.05; Table 4; Fig. 5i).

Table 4 Effects of leaf C_i:C_a, drivers of the cost to acquire nitrogen relative to water, and functional group on area-based leaf nitrogen content, mass-based leaf nitrogen content, and leaf mass per area*

	N_{area}				N_{mass}			M_{area}		
	df	Coefficient	χ^2	*p*	Coefficient	χ^2	*p*	Coefficient	χ^2	*p*
Intercept	-	$2.05*10^{0}$	-	-	$-2.08*10^{-3}$	-	-	$6.62*10^{0}$	-	-
Leaf C_i:C_a	1	$-1.68*10^{0}$	5.579	**0.018**	$8.51*10^{-1}$	0.127	0.722	$-2.55*10^{0}$	6.560	**0.010**
N availability (N)	1	$1.76*10^{-2}$	5.807	**0.016**	$1.12*10^{-2}$	82.829	**<0.001**	$-3.45*10^{-2}$	43.217	**<0.001**
Soil moisture (SM_{90})	1	$4.61*10^{-1}$	9.107	**0.003**	$8.15*10^{-1}$	5.094	**0.024**	$-3.74*10^{-1}$	0.538	0.463
PFT	2	-	40.208	**<0.001**	-	13.582	**0.001**	-	7.471	**0.024**
SM_{90} * N	1	$6.92*10^{-2}$	1.796	0.180	$-2.01*10^{-2}$	3.868	**0.049**	$1.07*10^{-1}$	0.091	0.763
Leaf C_i:C_a * PFT	2	-	23.869	**<0.001**	-	3.546	0.170	-	26.294	**<0.001**
N * PFT	2	-	6.138	**0.046**	-	1.702	0.427	-	16.622	**<0.001**
SM_{90} * PFT	2	-	1.354	0.508	-	1.721	0.423	-	0.454	0.797
SM_{90} * N * PFT	2	-	4.87	*0.088*	-	0.055	0.973	-	7.996	**0.018**

*Significance determined using Type II Wald χ^2 tests (α=0.05). *P*-values less than 0.05 are in bold and *p*-values where $0.05<p<0.1$ are italicized. Coefficients are reported on the natural-log scale for all response variables and are only included for continuous fixed effects. Key: df=degrees of freedom, χ^2=Wald Type II chi-square test statistic; N_{area}=area-based leaf nitrogen content (gN m^{-2}); N_{mass}=mass-based leaf nitrogen content (gN g^{-1}); leaf mass per area (M_{area}; g m^{-2})

497 **Figure 5**

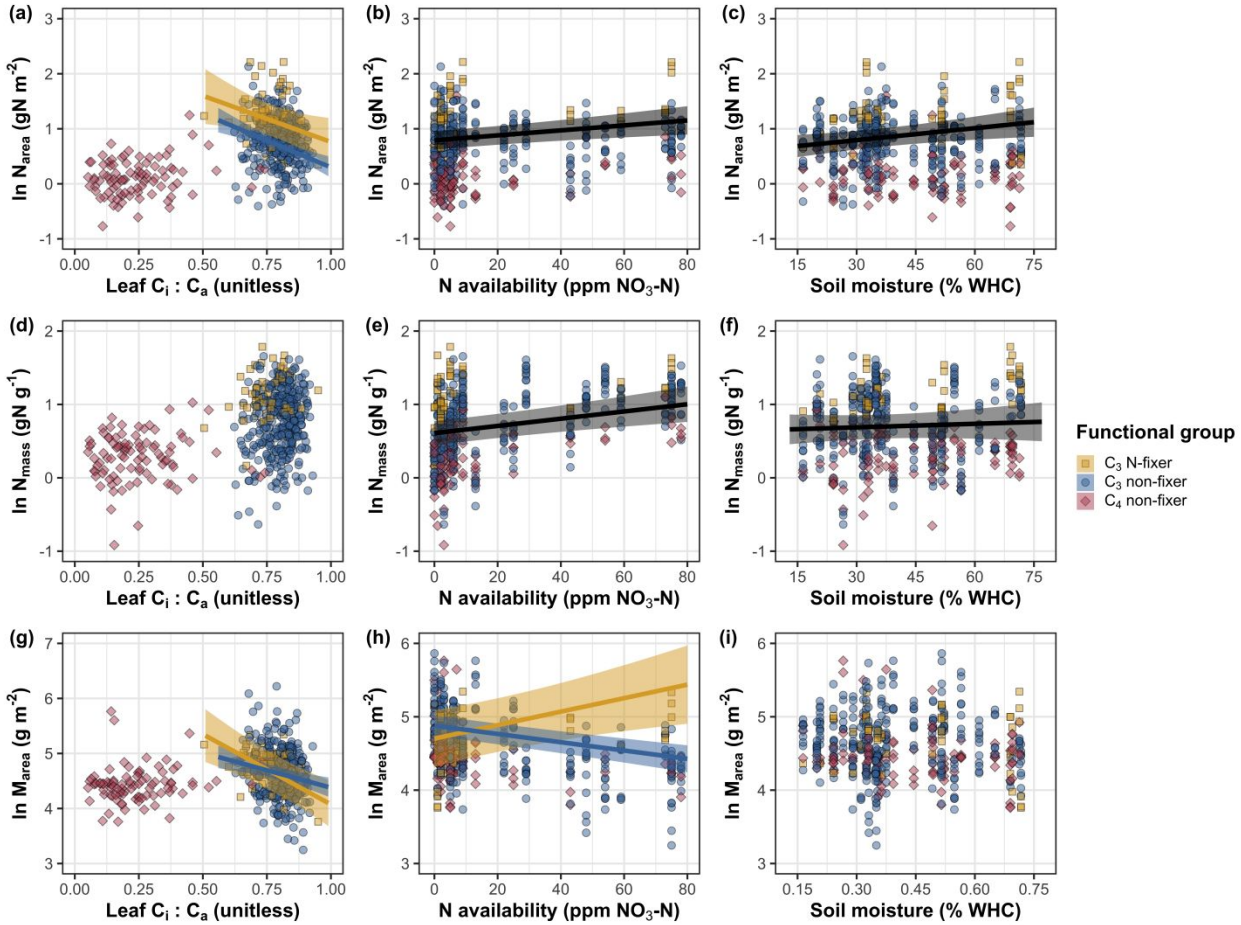

498

499 **Figure 5** Effects of leaf C_i:C_a, nitrogen availability, and soil moisture on area-based leaf nitrogen
500 content (a-c), mass-based leaf nitrogen content (d-f), and leaf mass per area (g-i). Colors, shapes,
501 and trendlines are as explained in Figure 3. All data are presented as natural-log transformed
502 values to normalize statistical model residuals. Trendlines are drawn using model predictions
503 using the 'emmeans' R package (Lenth 2019) across the range in x-axis values.

504

Structural equation model

Structural equation model results indicated that nitrogen availability decreased with increasing soil moisture, while soil moisture decreased with increasing VPD_{90} ($p<0.001$ in both cases; Table 5; Fig. 6). β increased with increasing nitrogen availability and decreased with increasing soil moisture, and was greater in C_3 species than C_4 species ($p<0.05$ in all cases; Table 5; Fig. 6) but was unrelated to ability to associate with symbiotic nitrogen-fixing bacteria ($p>0.05$; Table 5; Fig. 6). Leaf C_i:C_a decreased with increasing VPD_{90} and soil moisture, increased with increasing β, and was greater in C_3 species than C_4 species ($p<0.001$ in all cases; Table 5; Fig. 6). While N_{mass} was unrelated to leaf C_i:C_a ($p>0.05$; Table 5), N_{mass} decreased with increasing β, increased with increasing nitrogen availability, was greater in C_3 than C_4 species, and was greater in N-fixing than non-fixing species ($p<0.05$ in all cases; Table 5; Fig. 6). N_{mass} also exhibited strong negative covariance with M_{area} ($p<0.001$; Table 5; Fig. 6). M_{area} decreased with increasing leaf C_i:C_a and nitrogen availability and was greater in C_3 species than C_4 species ($p<0.05$ in all cases; Table 5; Fig. 6). Correlated error results indicated that VPD_{90} was negatively correlated with nitrogen availability ($p<0.001$; Table 5) and was unrelated to β ($p>0.05$; Table 5), while N_{mass} was unrelated to soil moisture ($p>0.05$; Table 5).

522 **Table 5** Structural equation model results investigating drivers of variance in area-based leaf
523 nitrogen content*

Predictor	Coefficient	*p*
***N*area**		
N_{mass}	0.899	**<0.001**
M_{area}	0.822	**<0.001**
***N*mass**		
Photo. pathway	-0.378	**0.004**
M_{area}	-0.373	**<0.001**
N-fixing ability	0.288	**<0.001**
Leaf C_i:C_a	0.185	0.154
β	-0.171	**0.012**
Soil N	0.166	**<0.001**
***M*area**		
Photo. pathway	-0.461	**0.010**
Leaf C_i:C_a	-0.309	**0.006**
Soil N	-0.255	**<0.001**
Leaf *C*i:*C*a		
Photo. pathway	-0.738	**<0.001**
β	0.316	**<0.001**
VPD_{90}	-0.096	**<0.001**
SM_{90}	-0.070	**<0.001**
β		
Photo. pathway	-0.816	**<0.001**
N-fixing ability	-0.114	0.189
SM_{90}	0.091	**0.005**
Soil N	-0.086	**0.002**
Soil N		
SM_{90}	-0.198	**<0.001**
Soil moisture		
VPD_{90}	-0.675	**<0.001**
Correlated Errors		
Soil N ~ VPD_{90}	-0.267	**<0.001**
N_{mass} ~ SM_{90}	-0.049	0.135
β ~ VPD_{90}	-0.062	0.080

524 *Coefficients, listed in order of magnitude for each predictor, are standardized across the
525 structural equation model. *P*-values less than 0.05 are in bold. Negative coefficients for
526 photosynthetic pathway indicate reduced values in C_4 species, while positive coefficients for N-
527 fixing ability indicate greater values in N-fixing species. Key: N_{area}=mass-based leaf nitrogen
528 content; N_{mass}=mass-based leaf nitrogen content (gN g^{-1}); M_{area}=leaf mass per leaf dry biomass (g
529 m^{-2}); *β*=cost of acquiring nitrogen relative to water (unitless); VPD_{90}=90-day mean vapor
530 pressure deficit (kPa); SM_{90}=90-day mean soil moisture as a function of water holding capacity

531 **Figure 6**

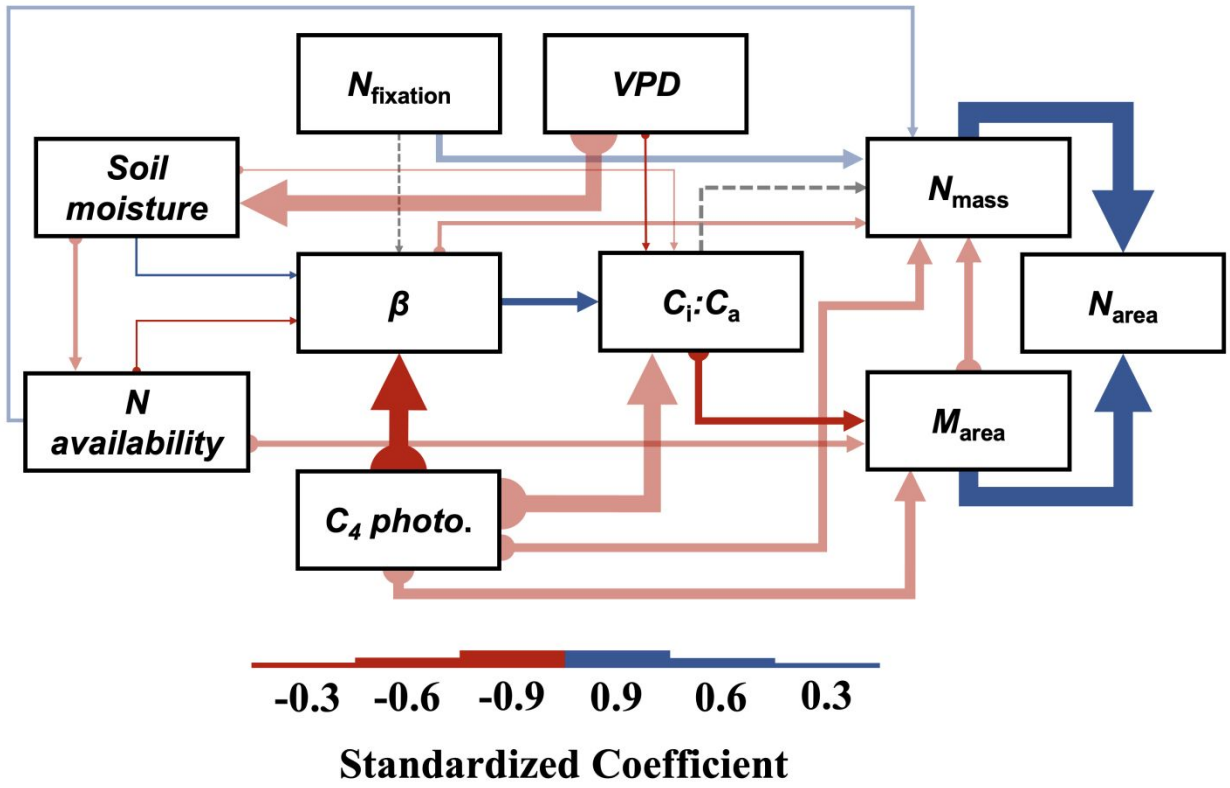

532

533 **Figure 6** Structural equation model results exploring drivers of variance in N_{area}. Boxes indicate
534 edaphic factors, climatic factors, and leaf traits. Solid arrows indicate significant bivariate
535 relationships (p<0.05) while dashed gray arrows indicate non-significant relationships (p>0.05).
536 Positive model coefficients are indicated through blue arrows while negative ones are indicated
537 through red, circular-anchored arrows. Arrow thickness scales with the standardized model
538 coefficient of each relationship. Transparent arrows indicate additional hypothesized
539 relationships not directly predicted by photosynthetic least-cost theory, while non-transparent
540 arrows indicate pathways predicted through patterns expected from the theory (Fig. 1). A
541 negative coefficient for photosynthetic pathway indicates reduced values in C_4 species, while a
542 positive coefficient for $N_{fixation}$ indicates larger values in N-fixing species.
543

Discussion

Direct and indirect effects of edaphic and climatic characteristics on N_{area} and components of N_{area} (N_{mass} and M_{area}) were quantified in 515 individuals spanning across an edaphic and climatic gradient in grasslands across Texas, USA. Patterns supporting photosynthetic least-cost theory emerged, a result driven by a negative relationship between leaf C_i:C_a and N_{area} mediated through a direct negative effect of increasing leaf C_i:C_a on M_{area}. In further support of the theory, increasing nitrogen availability was negatively associated with β, resulting in two pathways that contributed to an indirect positive effect of increasing nitrogen availability on N_{area}: (1) when mediated through a negative effect of increasing nitrogen availability on β, a positive relationship between β and leaf C_i:C_a, and negative effect of increasing leaf C_i:C_a on M_{area}, and (2) when mediated through a negative effect of increasing nitrogen availability on β and negative effect of increasing β on N_{mass}. Results indicated a third pathway where increasing nitrogen availability increased N_{area} directly through a larger increase in N_{mass} than decrease in M_{area} independent of changes in β or leaf C_i:C_a. Increasing soil moisture decreased N_{area} through positive relationships between soil moisture and β coupled with strong negative covariance between soil moisture and nitrogen availability, while increasing VPD_{90} increased N_{area} through negative effects of increasing VPD_{90} on leaf C_i:C_a.

Variance in leaf nitrogen content across the environmental gradient was the product of complex interactions between edaphic and climatic factors, most of which were capable of being predicted using theory. Interestingly, we observed substantial variability in β across the environmental gradient that was generally greater than the global mean value currently used in eco-evolutionary optimality models that adopt photosynthetic least-cost principles (e.g., the P-model; Stocker et al. 2020, Scott and Smith 2022). Findings from this study provide important insight into understanding drivers of variability in leaf nitrogen content across environmental gradients and suggest that optimality models may improve model simulations by including an approach for predicting β dynamically across environmental gradients (Wang et al. 2017, Lavergne et al. 2020, Paillassa et al. 2020).

Relationships between leaf C_i:C_a and N_{area} were driven by changes in leaf morphology

Negative relationships between leaf C_i:C_a and N_{area} are consistent with previous environmental gradient (Dong et al. 2017, Querejeta et al. 2022) and manipulation experiments (Perkowski et

al. *in review*), and supports nitrogen-water use tradeoffs expected from theory (Wright et al. 2003, Prentice et al. 2014). Negative covariance between leaf C_i:C_a and N_{area} was driven by negative effects of increasing leaf C_i:C_a on M_{area} paired with no relationship between leaf C_i:C_a and N_{mass}, suggesting that variance in leaf nitrogen content across the environmental gradient was driven by changes in leaf morphology rather than changes in leaf chemistry.

These results are consistent with patterns reported from previous studies indicating that variance in N_{area} is driven by M_{area} across environmental gradients and that part of this response is due to negative covariation between M_{area} and N_{mass} (Wright et al. 2004, Dong et al. 2017, 2022, Querejeta et al. 2022, Wang et al. 2023). Negative covariance between leaf C_i:C_a and M_{area} and between N_{mass} and M_{area} may be indicative of tradeoffs between leaf longevity and productivity, as increased M_{area} is often inferred to be the result of greater investment in cell wall tissue that helps promote greater leaf lifespan, while increased N_{mass} and leaf C_i:C_a are each commonly associated with greater photosynthetic capacity and increased leaf productivity (Onoda et al. 2004, 2017). Tradeoffs between leaf longevity and productivity form a dimension of trait variation known as the leaf economics spectrum, which places individuals along a spectrum of resource-use strategies ranging from fast-growing individuals with short leaf lifespans to slow-growing individuals with long leaf lifespans (Wright et al. 2004, Onoda et al. 2004, 2017, Reich 2014). These relationships support recent work suggesting that patterns observed in the leaf economics spectrum can be predicted across environmental gradients using patterns expected from photosynthetic least-cost theory (Wang et al. 2023).

Nitrogen availability increases N_{area} through multiple pathways

Mechanisms that explained positive effects of increasing nitrogen availability on leaf nitrogen content were multifaceted. Specifically, structural equation results indicated that nitrogen availability can have direct positive effects on N_{area} by increasing N_{mass}, following previous work (Firn et al. 2019, Liang et al. 2020), or can alternatively have indirect positive effects on N_{area} by either increased N_{mass} or M_{area} when mediated through reductions in the cost of acquiring nitrogen relative to water, following patterns observed in previous experiments (Eastman et al. 2021, Perkowski et al. 2021, Waring et al. 2023) and those expected from theory (Wright et al. 2003, Prentice et al. 2014, Paillassa et al. 2020). These findings suggest that patterns expected from theory can predict some, but not all, of the variance in N_{area} across nitrogen availability gradients,

606 as direct positive effects of nitrogen availability on N_{mass} are not expected from the theory unless
607 associated with a reduction in β. Whether positive responses of leaf nitrogen content to
608 increasing nitrogen availability mediated through changes in β and leaf C_i:C_a correspond with
609 enhanced with photosynthetic capacity, as suggested in Paillassa et al. (2020), remains an
610 important open question that should be addressed. Understanding relationships between nitrogen
611 availability, β, leaf nitrogen content, and photosynthetic capacity across environmental gradients
612 would provide useful insight toward understanding whether variance in leaf nitrogen content
613 across environmental gradients is the top-down product of climate-related changes in
614 photosynthetic capacity that alter demand to build and maintain photosynthetic enzymes (Smith
615 et al. 2019, Peng et al. 2021).
616
617 *Soil moisture effects on N_{area} follow theoretical expectations*
618 Increasing soil moisture had a positive effect on N_{area}, which linear mixed effect models
619 suggested was driven by a positive effect of increasing soil moisture on N_{mass} coupled with no
620 relationship between soil moisture and M_{area}. These patterns were observed in spite of a positive
621 effect of soil moisture on β, a response likely driven by a reduction in costs of water acquisition
622 (Wright et al. 2003, Prentice et al. 2014, Lavergne et al. 2020). While positive effects of
623 increasing soil moisture on β are consistent with theoretical expectations, theory predicts that
624 such responses should increase leaf C_i:C_a and decrease leaf nitrogen allocation. Structural
625 equation model results indicated two pathways where leaf C_i:C_a indirectly increased and N_{area}
626 decreased in response to increasing soil moisture: (1) a pathway where increasing soil moisture
627 increased β, β was positively related to leaf C_i:C_a, and leaf C_i:C_a was negatively related to M_{area},
628 and (2) a pathway where increasing soil moisture exhibited strong negative covariance with
629 nitrogen availability, leading to indirect decreases in N_{area} through negative effects of increasing
630 nitrogen availability on β. Interestingly, existence of the second pathway implies that effects of
631 soil moisture on N_{area} may have been more strongly driven by changes in nitrogen availability
632 than directly through changes in soil moisture.
633 Despite soil moisture responses to β that were directionally consistent with patterns
634 expected from theory, mechanisms governing variance in N_{area} across the soil moisture gradient
635 were multifaceted, as alternative pathways demonstrated indirect positive effects of soil moisture
636 on N_{area} mediated through direct effects of soil moisture on leaf C_i:C_a independent of β.

637 Regardless, results indicate that patterns expected from theory can explain some of the variance
638 in N_{area} across soil moisture gradients, following results from recent work (Lavergne et al. 2020,
639 Mengoli et al. 2023). Manipulative experiments that disentangle effects of soil moisture and
640 nitrogen availability on β, components of β (i.e., costs of acquiring nitrogen, costs of acquiring
641 water), leaf C_i:C_a, and components of N_{area} would help contextualize the mechanisms driving
642 these pathways.
643
644 *Indirect effects of VPD on N_{area} are mediated through leaf C_i:C_a*
645 Supporting theory, increasing *VPD* decreased leaf C_i:C_a, leading to an indirect increase in N_{area}
646 through increased M_{area}. These responses are consistent with previous work noting that
647 increasing VPD_{90} decreases stomatal conductance (Oren et al. 1999, Novick et al. 2016, Sulman
648 et al. 2016, Grossiord et al. 2020, López et al. 2021) and increases M_{area} (Wright et al. 2005, Li et
649 al. 2019), allowing plants to minimize water loss in response to increased atmospheric water
650 demand. Results also support findings from previous experiments across environmental
651 gradients, where increasing *VPD* increased N_{area} at reduced stomatal conductance (Dong et al.
652 2017, 2022, Paillassa et al. 2020, Westerband et al. 2023). Increasing N_{area} in response to
653 increasing VPD_{90} could allow plants to maximize photosynthetic capacity under reduced
654 stomatal conductance (Dong et al. 2022), though this pattern contrasts previous work suggesting
655 that long-term increases in *VPD* are associated with increased plant mortality, reduced net
656 primary productivity, and perhaps reductions in net photosynthesis rates over time due to
657 prolonged stomatal closure (Eamus et al. 2013, Yuan et al. 2019, Grossiord et al. 2020).
658 Importantly, negative effects of increasing *VPD* occur over longer timescales than was relevant
659 here. Our results could suggest that variance in N_{area} across the environmental gradient was an
660 acclimation response to aboveground climate, allowing plants to satisfy demand to build and
661 maintain photosynthetic enzymes and optimize photosynthetic processes by maximizing
662 resource-use efficiency (Paillassa et al. 2020, Peng et al. 2021, Dong et al. 2022, Westerband et
663 al. 2023). However, gas exchange data collected with concurrent measurements of resource
664 availability, β, leaf C_i:C_a, and leaf nitrogen content would be useful to test this conjecture.
665
666 *Species identity traits contributed to variance in β, leaf C_i:C_a, and leaf nitrogen content*

667 N-fixing species had greater N_{area} compared to non-fixing species, a pattern driven by greater
668 N_{mass} values in N-fixing species coupled with similar M_{area} values between N-fixing and non-
669 fixing species. Contrasting expectations, variance in β and leaf C_i:C_a across the environmental
670 gradient was unrelated to N-fixing ability. These results support previous studies indicating that
671 increased N_{area} in N-fixing species is not consistently correlated with stronger increases in water-
672 use efficiency or reductions in leaf C_i:C_a compared to non-fixing species (Adams et al. 2016,
673 Dong et al. 2017, Bytnerowicz et al. 2023). These results do not support our hypothesis or
674 theoretical expectations, where increased N_{area} in N-fixing species is expected to be driven by a
675 reduction in β and leaf C_i:C_a relative to non-fixing species. Instead, greater N_{area} values in N-
676 fixing species were driven by a direct increase in N_{mass} that was independent of β and leaf C_i:C_a.
677 This response could be due to additional costs of nitrogen fixation, as it is energetically
678 expensive to maintain mutualistic relationships with symbiotic nitrogen-fixing bacteria.
679 C_4 species had reduced β, leaf C_i:C_a, and N_{area} compared to C_3 species, supporting our
680 hypotheses and some theoretical expectations. Reduced β values in C_4 non-fixers could have
681 been due to reduced costs of nitrogen acquisition and/or increased costs of water acquisition
682 (Wright et al. 2003, Prentice et al. 2014). These patterns may have been driven by reduced costs
683 of nitrogen acquisition, in part because increased nitrogen-use efficiency in C_4 species may
684 reduce demand to acquire nitrogen and therefore reduce associated costs of acquiring and using
685 nitrogen. However, this mechanism is not easily identifiable with this dataset because β was
686 calculated using isotope-derived leaf C_i:C_a, which is itself reduced in C_4 species. Future work
687 should consider quantifying costs of nitrogen acquisition and costs of water acquisition
688 separately to assess which component drives changes in β across functional groups and
689 environmental gradients.
690 Reduced N_{area} in C_4 species follow findings from previous studies (Schmitt and Edwards
691 1981, Sage and Pearcy 1987, Ghannoum et al. 2011), though these patterns were not driven by
692 negative relationships between leaf C_i:C_a and N_{area} as expected from theory. Instead, N_{area} and
693 leaf C_i:C_a were each reduced in C_4 species compared to both C_3 functional groups. These
694 patterns could suggest that C_4 species had increased nitrogen-use efficiency compared to either
695 C_3 functional group, which could be driven by increased Rubisco carboxylation efficiency
696 associated with CO_2 concentrating mechanisms that reduces photorespiration (Ghannoum et al.
697 2011). Increased nitrogen-use efficiency at the leaf level could reduce or eliminate the need to

sacrifice inefficient nitrogen use for efficient water use to achieve optimal photosynthesis rates, which may explain why reduced N_{area} in C_4 species was not associated with increased leaf C_i:C_a.

Implications for least-cost optimality model development

Optimality models have been developed for C_3 and C_4 species using photosynthetic least-cost principles (Prentice et al. 2014, Wang et al. 2017, Smith et al. 2019, Stocker et al. 2020, Scott and Smith 2022). These optimality models hold β constant using a global dataset of leaf $\delta^{13}C$ (Wang et al. 2017, Cornwell et al. 2018), where C_3 optimality models assume either a constant β of 240 (Wang et al. 2017) or 146 (Stocker et al. 2020), while the C_4 optimality model assumes a constant β of 166 (Scott and Smith 2022). Across functional groups, our results indicate that β ranged from 33.9 to 714.5 in C_3 N-fixers (mean: 209.3; median: 187.7; standard deviation: 147.4), from 15.7 to 1821.1 in C_3 non-fixers (mean: 426.4; median: 346.2; standard deviation: 315.6), and from <0.1 to 362.7 in C_4 non-fixers (mean: 19.6; median: 0.9; standard deviation: 59.4). The high degree of β variability within functional groups across the environmental gradient suggests that the use of single parameterized β values within C_3/C_4 functional groups may contribute to errors in optimality model simulations.

In this study, β in C_3 species was, on average, greater than the global mean value currently included in optimality models, suggesting that individuals in these systems had greater costs of acquiring nitrogen and/or reduced costs of acquiring water relative to the global mean. Interestingly, β in C_4 species was, on average, less than the current parameterized global value, indicating that individuals had reduced costs of acquiring nitrogen and/or greater costs of acquiring water relative to the global mean. As mentioned above, mechanisms driving these responses are unclear as we are unable to identify components of β when it is calculated using carbon isotope data. Thus, future work should investigate mechanisms driving β variability across environmental gradients by quantifying costs of nitrogen acquisition and costs of water acquisition separately.

Conclusions

We evaluated direct and indirect drivers of N_{area} across an environmental gradient in Texas grasslands, finding that N_{area} was the product of complex interactions between climate and soil resource availability. Results indicate patterns supportive of those expected from photosynthetic

729 least-cost theory. Specifically, effects of aboveground climate on N_{area} were mediated by
730 negative relationships between M_{area} and leaf C_i:C_a, while effects of nitrogen availability and soil
731 moisture on N_{area} were mediated by β and, in some cases, negative relationships between M_{area}
732 and leaf C_i:C_a. We found that the theory could predict impacts of photosynthetic pathway on
733 variance in β and leaf C_i:C_a across the environmental gradient; however, found that leaf nitrogen
734 content in C_4 species was unrelated to leaf C_i:C_a, contrasting theoretical expectations. Patterns
735 expected from theory were not modified by N-fixing ability, though N-fixing species did
736 generally have greater N_{area} than non-fixing species. Interestingly, β varied substantially across
737 the environmental gradient despite generally increasing with increasing soil moisture and
738 decreasing with increasing nitrogen availability, suggesting that future iterations of optimality
739 models that adopt photosynthetic least-cost principles may consider implementing frameworks
740 where β is calculated dynamically. Overall, results from this environmental gradient experiment
741 show that photosynthetic least-cost theory is capable of predicting much of the variability in leaf
742 nitrogen content across climatic and edaphic gradients, building on previous claims that the
743 theory may be suitable for implementation in terrestrial biosphere models.
744

745 **References**

746 Adams, M. A., T. L. Turnbull, J. I. Sprent, and N. Buchmann. 2016. Legumes are different: Leaf
747 nitrogen, photosynthesis, and water use efficiency. Proceedings of the National Academy of
748 Sciences of the United States of America 113:4098–4103.
749 Bates, D., M. Mächler, B. Bolker, and S. Walker. 2015. Fitting linear mixed-effects models using
750 lme4. Journal of Statistical Software 67:1–48.
751 Bernacchi, C. J., E. L. Singsaas, C. Pimentel, A. R. Portis Jr, and S. P. Long. 2001. Improved
752 temperature response functions for models of Rubisco-limited photosynthesis. Plant, Cell &
753 Environment 24:253–259.
754 Bloomfield, K. J., B. D. Stocker, T. F. Keenan, and I. C. Prentice. 2022. Environmental controls
755 on the light use efficiency of terrestrial gross primary production. Global Change
756 Biology:0–2.
757 Booth, B. B. B., C. D. Jones, M. Collins, I. J. Totterdell, P. M. Cox, S. Sitch, C. Huntingford, R.
758 A. Betts, G. R. Harris, and J. Lloyd. 2012. High sensitivity of future global warming to land
759 carbon cycle processes. Environmental Research Letters 7:024002.
760 Braghiere, R. K., J. B. Fisher, K. Allen, E. R. Brzostek, M. Shi, X. Yang, D. M. Ricciuto, R. A.
761 Fisher, Q. Zhu, and R. P. Phillips. 2022. Modeling Global Carbon Costs of Plant Nitrogen
762 and Phosphorus Acquisition. Journal of Advances in Modeling Earth Systems 14:1–23.
763 Brzostek, E. R., D. Dragoni, H. P. Schmid, A. F. Rahman, D. Sims, C. A. Wayson, D. J.
764 Johnson, and R. P. Phillips. 2014. Chronic water stress reduces tree growth and the carbon
765 sink of deciduous hardwood forests. Global Change Biology 20:2531–2539.
766 Bytnerowicz, T. A., J. L. Funk, D. N. L. Menge, S. S. Perakis, and A. A. Wolf. 2023. Leaf
767 nitrogen affects photosynthesis and water use efficiency similarly in nitrogen-fixing and
768 non-fixing trees. Journal of Ecology:1–15.
769 Cornwell, W. K., I. J. Wright, J. Turner, V. Maire, M. M. Barbour, L. A. Cernusak, T. E.
770 Dawson, D. S. Ellsworth, G. D. Farquhar, H. Griffiths, C. Keitel, A. Knohl, P. B. Reich, D.
771 G. Williams, R. Bhaskar, J. H. C. Cornelissen, A. Richards, S. Schmidt, F. Valladares, C.
772 Körner, E.-D. Schulze, N. Buchmann, and L. S. Santiago. 2018. Climate and soils together
773 regulate photosynthetic carbon isotope discrimination within C_3 plants worldwide. Global
774 Ecology and Biogeography 27:1056–1067.
775 Cramer, W., and I. C. Prentice. 1988. Simulation of regional soil moisture deficits on a European

776 scale. Norsk Geografisk Tidsskrift - Norwegian Journal of Geography 42:149–151.
777 Daly, C., M. Halbleib, J. I. Smith, W. P. Gibson, M. K. Doggett, G. H. Taylor, J. Curtis, and P.
778 P. Pasteris. 2008. Physiographically sensitive mapping of climatological temperature and
779 precipitation across the conterminous United States. International Journal of Climatology
780 28:2031–2064.
781 Davies-Barnard, T., J. Meyerholt, S. Zaehle, P. Friedlingstein, V. Brovkin, Y. Fan, R. A. Fisher,
782 C. D. Jones, H. Lee, D. Peano, B. Smith, D. Wårlind, and A. J. Wiltshire. 2020. Nitrogen
783 cycling in CMIP6 land surface models: progress and limitations. Biogeosciences 17:5129–
784 5148.
785 Davis, T. W., I. C. Prentice, B. D. Stocker, R. T. Thomas, R. J. Whitley, H. Wang, B. J. Evans,
786 A. V Gallego-Sala, M. T. Sykes, and W. Cramer. 2017. Simple process-led algorithms for
787 simulating habitats (SPLASH v.1.0): robust indices of radiation, evapotranspiration and
788 plant-available moisture. Geoscientific Model Development 10:689–708.
789 Dong, N., I. C. Prentice, B. J. Evans, S. Caddy-Retalic, A. J. Lowe, and I. J. Wright. 2017. Leaf
790 nitrogen from first principles: field evidence for adaptive variation with climate.
791 Biogeosciences 14:481–495.
792 Dong, N., I. C. Prentice, I. J. Wright, B. J. Evans, H. F. Togashi, S. Caddy-Retalic, F. A.
793 McInerney, B. Sparrow, E. Leitch, and A. J. Lowe. 2020. Components of leaf-trait variation
794 along environmental gradients. New Phytologist 228:82–94.
795 Dong, N., I. C. Prentice, I. J. Wright, H. Wang, O. K. Atkin, K. J. Bloomfield, T. F. Domingues,
796 S. M. Gleason, V. Maire, Y. Onoda, H. Poorter, and N. G. Smith. 2022. Leaf nitrogen from
797 the perspective of optimal plant function. Journal of Ecology 110:2585–2602.
798 Eamus, D., N. Boulain, J. Cleverly, and D. D. Breshears. 2013. Global change-type drought-
799 induced tree mortality: Vapor pressure deficit is more important than temperature per se in
800 causing decline in tree health. Ecology and Evolution 3:2711–2729.
801 Eastman, B. A., M. B. Adams, E. R. Brzostek, M. B. Burnham, J. E. Carrara, C. Kelly, B. E.
802 McNeil, C. A. Walter, and W. T. Peterjohn. 2021. Altered plant carbon partitioning
803 enhanced forest ecosystem carbon storage after 25 years of nitrogen additions. New
804 Phytologist 230:1435–1448.
805 Evans, J. R. 1989a. Partitioning of nitrogen between and within leaves grown under different
806 irradiances. Functional Plant Biology 16:533.

807 Evans, J. R. 1989b. Photosynthesis and nitrogen relationships in leaves of C_3 plants. Oecologia
808 78:9–19.
809 Evans, J. R., and J. R. Seemann. 1989. The allocation of protein nitrogen in the photosynthetic
810 apparatus: costs, consequences, and control. Photosynthesis 8:183–205.
811 Farquhar, G. D., J. R. Ehleringer, and K. T. Hubick. 1989. Carbon Isotope Discrimination and
812 Photosynthesis. Annual Review of Plant Physiology and Plant Molecular Biology 40:503–
813 537.
814 Fay, P. A., S. M. Prober, W. S. Harpole, J. M. H. Knops, J. D. Bakker, E. T. Borer, E. M. Lind,
815 A. S. MacDougall, E. W. Seabloom, P. D. Wragg, P. B. Adler, D. M. Blumenthal, Y. M.
816 Buckley, C. Chu, E. E. Cleland, S. L. Collins, K. F. Davies, G. Du, X. Feng, J. Firn, D. S.
817 Gruner, N. Hagenah, Y. Hautier, R. W. Heckman, V. L. Jin, K. P. Kirkman, J. A. Klein, L.
818 M. Ladwig, Q. Li, R. L. McCulley, B. A. Melbourne, C. E. Mitchell, J. L. Moore, J. W.
819 Morgan, A. C. Risch, M. Schütz, C. J. Stevens, D. A. Wedin, and L. H. Yang. 2015.
820 Grassland productivity limited by multiple nutrients. Nature Plants 1:15080.
821 Field, C. B., and H. A. Mooney. 1986. The photosynthesis-nitrogen relationship in wild plants.
822 Pages 25–55 *in* T. J. Givnish, editor. On the Economy of Plant Form and Function.
823 Cambridge University Press, Cambridge.
824 Firn, J., J. M. McGree, E. Harvey, H. Flores-Moreno, M. Schütz, Y. M. Buckley, E. T. Borer, E.
825 W. Seabloom, K. J. La Pierre, A. M. MacDougall, S. M. Prober, C. J. Stevens, L. L.
826 Sullivan, E. Porter, E. Ladouceur, C. Allen, K. H. Moromizato, J. W. Morgan, W. S.
827 Harpole, Y. Hautier, N. Eisenhauer, J. P. Wright, P. B. Adler, C. A. Arnillas, J. D. Bakker,
828 L. Biederman, A. A. D. Broadbent, C. S. Brown, M. N. Bugalho, M. C. Caldeira, E. E.
829 Cleland, A. Ebeling, P. A. Fay, N. Hagenah, A. R. Kleinhesselink, R. Mitchell, J. L. Moore,
830 C. Nogueira, P. L. Peri, C. Roscher, M. D. Smith, P. D. Wragg, and A. C. Risch. 2019. Leaf
831 nutrients, not specific leaf area, are consistent indicators of elevated nutrient inputs. Nature
832 Ecology & Evolution 3:400–406.
833 Fox, J., and S. Weisberg. 2019. An R companion to applied regression. Third edit. Sage,
834 Thousand Oaks, California.
835 Friel, C. A., and M. L. Friesen. 2019. Legumes modulate allocation to rhizobial nitrogen fixation
836 in response to factorial light and nitrogen manipulation. Frontiers in Plant Science 10:1316.
837 Ghannoum, O., J. R. Evans, and S. von Caemmerer. 2011. Nitrogen and water use efficiency of

C4 plants. Pages 129–146 *in* A. S. Raghavendra and R. F. Sage, editors. C4 Photosynthesis and Related CO2 Concentrating Mechanisms. Springer.

Grossiord, C., T. N. Buckley, L. A. Cernusak, K. A. Novick, B. Poulter, R. T. W. Siegwolf, J. S. Sperry, and N. G. McDowell. 2020. Plant responses to rising vapor pressure deficit. New Phytologist 226:1550–1566.

Hijmans, R. J. 2022. terra: Spatial Data Analysis.

Huber, M. L., R. A. Perkins, A. Laesecke, D. G. Friend, J. V Sengers, M. J. Assael, I. N. Metaxa, E. Vogel, R. Mareš, and K. Miyagawa. 2009. New international formulation for the viscosity of H2 O. Journal of Physical and Chemical Reference Data 38:101–125.

Hungate, B. A., J. S. Dukes, M. R. Shaw, Y. Luo, and C. B. Field. 2003. Nitrogen and climate change. Science 302:1512–1513.

IPCC. 2021. Climate Change 2021: The Physical Science Basis. Contribution of Working Group I to the Sixth Assessment Report of the Intergovernmental Panel on Climate Change. Page (V. Masson-Delmotte, P. Zhai, A. Pirani, S. L. Connors, S. Berger, N. Caud, Y. Chen, L. Goldfarb, M. I. Gomis, M. Huang, K. Leitzell, E. Lonnoy, J. B. R. Matthews, T. K. Maycock, T. Waterfield, O. Yelekçi, R. Yu, and B. Zhou, Eds.). Cambridge University Press, Cambridge, UK and New York, USA.

Kachurina, O. M., H. Zhang, W. R. Raun, and E. G. Krenzer. 2000. Simultaneous determination of soil aluminum, ammonium- and nitrate- nitrogen using 1 M potassium chloride. Communications in Soil Science and Plant Analysis 31:893–903.

Katabuchi, M. 2015. LeafArea: An R package for rapid digital analysis of leaf area. Ecological Research 30:1073–1077.

Kattge, J., W. Knorr, T. Raddatz, and C. Wirth. 2009. Quantifying photosynthetic capacity and its relationship to leaf nitrogen content for global-scale terrestrial biosphere models. Global Change Biology 15:976–991.

Keeney, D. R., and D. W. Nelson. 1983. Nitrogen—Inorganic Forms. Pages 643–698 *in* A. L. Page, editor. Methods of Soil Analysis. 2nd edition. ASA and SSSA, Madison, WI, USA.

Kenward, M. G., and J. H. Roger. 1997. Small Sample Inference for Fixed Effects from Restricted Maximum Likelihood. Biometrics 53:983.

Knorr, W., and M. Heimann. 2001. Uncertainties in global terrestrial biosphere modeling: 1. A comprehensive sensitivity analysis with a new photosynthesis and energy balance scheme.

Global Biogeochemical Cycles 15:207–225.

Lavergne, A., D. Sandoval, V. J. Hare, H. Graven, and I. C. Prentice. 2020. Impacts of soil water stress on the acclimated stomatal limitation of photosynthesis: Insights from stable carbon isotope data. Global Change Biology 26:7158–7172.

Lawrence, D. M., R. A. Fisher, C. D. Koven, K. W. Oleson, S. C. Swenson, G. B. Bonan, N. Collier, B. Ghimire, L. Kampenhout, D. Kennedy, E. Kluzek, P. J. Lawrence, F. Li, H. Li, D. L. Lombardozzi, W. J. Riley, W. J. Sacks, M. Shi, M. Vertenstein, W. R. Wieder, C. Xu, A. A. Ali, A. M. Badger, G. Bisht, M. Broeke, M. A. Brunke, S. P. Burns, J. Buzan, M. Clark, A. Craig, K. M. Dahlin, B. Drewniak, J. B. Fisher, M. Flanner, A. M. Fox, P. Gentine, F. M. Hoffman, G. Keppel-Aleks, R. Knox, S. Kumar, J. Lenaerts, L. R. Leung, W. H. Lipscomb, Y. Lu, A. Pandey, J. D. Pelletier, J. Perket, J. T. Randerson, D. M. Ricciuto, B. M. Sanderson, A. Slater, Z. M. Subin, J. Tang, R. Q. Thomas, M. Val Martin, and X. Zeng. 2019. The Community Land Model Version 5: description of new features, benchmarking, and impact of forcing uncertainty. Journal of Advances in Modeling Earth Systems 11:4245–4287.

LeBauer, D. S., and K. Treseder. 2008. Nitrogen limitation of net primary productivity in terrestrial ecosystems is globally distributed. Ecology 89:371–379.

Lefcheck, J. S. 2016. piecewiseSEM: Piecewise structural equation modelling in r for ecology, evolution, and systematics. Methods in Ecology and Evolution 7:573–579.

Lenth, R. 2019. emmeans: estimated marginal means, aka least-squares means.

Li, Q., M. Wei, Y. Li, G. Feng, Y. Wang, S. Li, and D. Zhang. 2019. Effects of soil moisture on water transport, photosynthetic carbon gain and water use efficiency in tomato are influenced by evaporative demand. Agricultural Water Management 226.

Li, W., H. Zhang, G. Huang, R. Liu, H. Wu, C. Zhao, and N. G. McDowell. 2020. Effects of nitrogen enrichment on tree carbon allocation: A global synthesis. Global Ecology and Biogeography 29:573–589.

Liang, X., T. Zhang, X. Lu, D. S. Ellsworth, H. BassiriRad, C. You, D. Wang, P. He, Q. Deng, H. Liu, J. Mo, and Q. Ye. 2020. Global response patterns of plant photosynthesis to nitrogen addition: A meta-analysis. Global Change Biology 26:3585–3600.

López, J., D. A. Way, and W. Sadok. 2021. Systemic effects of rising atmospheric vapor pressure deficit on plant physiology and productivity. Global Change Biology 27:1704–

1720.

Luo, X., T. F. Keenan, J. M. Chen, H. Croft, I. C. Prentice, N. G. Smith, A. P. Walker, H. Wang, R. Wang, C. Xu, and Y. Zhang. 2021. Global variation in the fraction of leaf nitrogen allocated to photosynthesis. Nature Communications 12:4866.

Mengoli, G., S. P. Harrison, and I. C. Prentice. 2023. A global function of climatic aridity accounts for soil moisture stress on carbon assimilation. EGUsphere.

Novick, K. A., D. L. Ficklin, P. C. Stoy, C. A. Williams, G. Bohrer, A. C. Oishi, S. A. Papuga, P. D. Blanken, A. Noormets, B. N. Sulman, R. L. Scott, L. Wang, and R. P. Phillips. 2016. The increasing importance of atmospheric demand for ecosystem water and carbon fluxes. Nature Climate Change 6:1023–1027.

Onoda, Y., K. Hikosaka, and T. Hirose. 2004. Allocation of nitrogen to cell walls decreases photosynthetic nitrogen-use efficiency. Functional Ecology 18:419–425.

Onoda, Y., I. J. Wright, J. R. Evans, K. Hikosaka, K. Kitajima, Ü. Niinemets, H. Poorter, T. Tosens, and M. Westoby. 2017. Physiological and structural tradeoffs underlying the leaf economics spectrum. New Phytologist 214:1447–1463.

Oren, R., J. S. Sperry, G. G. Katul, D. E. Pataki, B. E. Ewers, N. Phillips, and K. V. R. Schäfer. 1999. Survey and synthesis of intra- and interspecific variation in stomatal sensitivity to vapour pressure deficit. Plant, Cell and Environment 22:1515–1526.

Paillassa, J., I. J. Wright, I. C. Prentice, S. Pepin, N. G. Smith, G. Ethier, A. C. Westerband, L. J. Lamarque, H. Wang, W. K. Cornwell, and V. Maire. 2020. When and where soil is important to modify the carbon and water economy of leaves. New Phytologist 228:121–135.

Peng, Y., K. J. Bloomfield, L. A. Cernusak, T. F. Domingues, and I. C. Prentice. 2021. Global climate and nutrient controls of photosynthetic capacity. Communications Biology 4:462.

Perkowski, E. A., D. W. Frey, C. L. Goodale, and N. G. Smith. (n.d.). Increasing nitrogen availability increases water use efficiency and decreases nitrogen use efficiency in *Acer saccharum*: a test of photosynthetic least-cost theory in mature forests.

Perkowski, E. A., E. F. Waring, and N. G. Smith. 2021. Root mass carbon costs to acquire nitrogen are determined by nitrogen and light availability in two species with different nitrogen acquisition strategies. Journal of Experimental Botany 72:5766–5776.

Pinheiro, J., and D. Bates. 2022. nlme: linear and nonlinear mixed effects models.

931 Poorter, H., Ü. Niinemets, L. Poorter, I. J. Wright, and R. Villar. 2009. Causes and consequences
932 of variation in leaf mass per area (LMA): A meta-analysis. New Phytologist 182:565–588.
933 Prentice, I. C., N. Dong, S. M. Gleason, V. Maire, and I. J. Wright. 2014. Balancing the costs of
934 carbon gain and water transport: testing a new theoretical framework for plant functional
935 ecology. Ecology Letters 17:82–91.
936 Priestley, C. H. B., and R. J. Taylor. 1972. On the Assessment of Surface Heat Flux and
937 Evaporation Using Large-Scale Parameters. Monthly Weather Review 100:81–92.
938 Querejeta, J. I., I. Prieto, C. Armas, F. Casanoves, J. S. Diémé, M. Diouf, H. Yossi, B. Kaya, F. I.
939 Pugnaire, and G. M. Rusch. 2022. Higher leaf nitrogen content is linked to tighter stomatal
940 regulation of transpiration and more efficient water use across dryland trees. New
941 Phytologist 235:1351–1364.
942 R Core Team. 2021. R: A language and environment for statistical computing. R Foundation for
943 Statistical Computing, Vienna, Austria.
944 Reich, P. B. 2014. The world-wide 'fast-slow' plant economics spectrum: a traits manifesto.
945 Journal of Ecology 102:275–301.
946 Reynolds, J. F., D. M. Stafford Smith, E. F. Lambin, B. L. Turner, M. Mortimore, S. P. J.
947 Batterbury, T. E. Downing, H. Dowlatabadi, R. J. Fernández, J. E. Herrick, E. Huber-
948 Sannwald, H. Jiang, R. Leemans, T. Lynam, F. T. Maestre, M. Ayarza, and B. Walker.
949 2007. Ecology: Global desertification: Building a science for dryland development. Science
950 316:847–851.
951 Rogers, A. 2014. The use and misuse of $V_{c,max}$ in Earth System Models. Photosynthesis Research
952 119:15–29.
953 Rogers, A., B. E. Medlyn, J. S. Dukes, G. B. Bonan, S. Caemmerer, M. C. Dietze, J. Kattge, A.
954 D. B. Leakey, L. M. Mercado, Ü. Niinemets, I. C. Prentice, S. P. Serbin, S. Sitch, D. A.
955 Way, and S. Zaehle. 2017. A roadmap for improving the representation of photosynthesis in
956 Earth system models. New Phytologist 213:22–42.
957 Sage, R. F., and R. W. Pearcy. 1987. The nitrogen use efficiency of C3 and C4 plants: I. Leaf
958 nitrogen, growth, and biomass partitioning in *Chenopodium album* (L.) and *Amaranthus*
959 *retroflexus* (L.). Plant Physiology 84:954–958.
960 Saxton, K. E., and W. J. Rawls. 2006. Soil water characteristic estimates by texture and organic
961 matter for hydrologic solutions. Soil Science Society of America Journal 70:1569–1578.

962 Schmitt, M. R., and G. E. Edwards. 1981. Photosynthetic capacity and nitrogen use efficiency of
963 maize, wheat, and rice: A comparison between C3 and C4 photosynthesis. Journal of
964 Experimental Botany 32:459–466.
965 Schneider, C. A., W. S. Rasband, and K. W. Eliceiri. 2012. NIH Image to ImageJ: 25 years of
966 image analysis. Nature methods 9:671–675.
967 Scott, H. G., and N. G. Smith. 2022. A Model of C4 Photosynthetic Acclimation Based on Least-
968 Cost Optimality Theory Suitable for Earth System Model Incorporation. Journal of
969 Advances in Modeling Earth Systems 14:1–16.
970 Shi, M., J. B. Fisher, E. R. Brzostek, and R. P. Phillips. 2016. Carbon cost of plant nitrogen
971 acquisition: Global carbon cycle impact from an improved plant nitrogen cycle in the
972 Community Land Model. Global Change Biology 22:1299–1314.
973 Smith, B., D. Wärlind, A. Arneth, T. Hickler, P. Leadley, J. Siltberg, and S. Zaehle. 2014.
974 Implications of incorporating N cycling and N limitations on primary production in an
975 individual-based dynamic vegetation model. Biogeosciences 11:2027–2054.
976 Smith, N. G., T. F. Keenan, I. C. Prentice, H. Wang, I. J. Wright, Ü. Niinemets, K. Y. Crous, T.
977 F. Domingues, R. Guerrieri, F. oko Ishida, J. Kattge, E. L. Kruger, V. Maire, A. Rogers, S.
978 P. Serbin, L. Tarvainen, H. F. Togashi, P. A. Townsend, M. Wang, L. K. Weerasinghe, and
979 S.-X. Zhou. 2019. Global photosynthetic capacity is optimized to the environment. Ecology
980 Letters 22:506–517.
981 Stocker, B. D., H. Wang, N. G. Smith, S. P. Harrison, T. F. Keenan, D. Sandoval, T. Davis, and
982 I. C. Prentice. 2020. P-model v1.0: An optimality-based light use efficiency model for
983 simulating ecosystem gross primary production. Geoscientific Model Development
984 13:1545–1581.
985 Stocker, B. D., J. Zscheischler, T. F. Keenan, I. C. Prentice, J. Peñuelas, and S. I. Seneviratne.
986 2018. Quantifying soil moisture impacts on light use efficiency across biomes. New
987 Phytologist 218:1430–1449.
988 Sulman, B. N., D. T. Roman, K. Yi, L. Wang, R. P. Phillips, and K. A. Novick. 2016. High
989 atmospheric demand for water can limit forest carbon uptake and transpiration as severely
990 as dry soil. Geophysical Research Letters 43:9686–9695.
991 Taylor, B. N., and D. N. L. Menge. 2018. Light regulates tropical symbiotic nitrogen fixation
992 more strongly than soil nitrogen. Nature Plants 4:655–661.

993 Thieurmel, B., and A. Elmarhraoui. 2019. suncalc: Compute sun position, sunlight phases, moon
994 position, and lunar phase.
995 Walker, A. P., A. P. Beckerman, L. Gu, J. Kattge, L. A. Cernusak, T. F. Domingues, J. C. Scales,
996 G. Wohlfahrt, S. D. Wullschleger, and F. I. Woodward. 2014. The relationship of leaf
997 photosynthetic traits - Vcmax and Jmax - to leaf nitrogen, leaf phosphorus, and specific leaf
998 area: a meta-analysis and modeling study. Ecology and Evolution 4:3218–3235.
999 Walker, A. P., A. L. Johnson, A. Rogers, J. Anderson, R. A. Bridges, R. A. Fisher, D. Lu, D. M.
1000 Ricciuto, S. P. Serbin, and M. Ye. 2021. Multi-hypothesis comparison of Farquhar and
1001 Collatz photosynthesis models reveals the unexpected influence of empirical assumptions at
1002 leaf and global scales. Global Change Biology 27:804–822.
1003 Wang, H., I. C. Prentice, T. F. Keenan, T. W. Davis, I. J. Wright, W. K. Cornwell, B. J. Evans,
1004 and C. Peng. 2017. Towards a universal model for carbon dioxide uptake by plants. Nature
1005 Plants 3:734–741.
1006 Wang, H., I. C. Prentice, I. J. Wright, D. I. Warton, S. Qiao, X. Xu, J. Zhou, K. Kikuzawa, and
1007 N. C. Stenseth. 2023. Leaf economics fundamentals explained by optimality principles.
1008 Science Advances 9:eadd566.
1009 Waring, E. F., E. A. Perkowski, and N. G. Smith. 2023. Soil nitrogen fertilization reduces
1010 relative leaf nitrogen allocation to photosynthesis. Journal of Experimental Botany
1011 74:5166–5180.
1012 Westerband, A. C., I. J. Wright, V. Maire, J. Paillassa, I. C. Prentice, O. K. Atkin, K. J.
1013 Bloomfield, L. A. Cernusak, N. Dong, S. M. Gleason, C. Guilherme Pereira, H. Lambers,
1014 M. R. Leishman, Y. Malhi, and R. H. Nolan. 2023. Coordination of photosynthetic traits
1015 across soil and climate gradients. Global Change Biology 29:856–873.
1016 Wieder, W. R., C. C. Cleveland, W. K. Smith, and K. Todd-Brown. 2015. Future productivity
1017 and carbon storage limited by terrestrial nutrient availability. Nature Geoscience 8:441–444.
1018 Wright, I. J., P. B. Reich, J. H. C. Cornelissen, D. S. Falster, P. K. Groom, K. Hikosaka, W. Lee,
1019 C. H. Lusk, Ü. Niinemets, J. Oleksyn, N. Osada, H. Poorter, D. I. Warton, and M. Westoby.
1020 2005. Modulation of leaf economic traits and trait relationships by climate. Global Ecology
1021 and Biogeography 14:411–421.
1022 Wright, I. J., P. B. Reich, and M. Westoby. 2003. Least-cost input mixtures of water and nitrogen
1023 for photosynthesis. The American Naturalist 161:98–111.

Wright, I. J., P. B. Reich, M. Westoby, D. D. Ackerly, Z. Baruch, F. Bongers, J. Cavender-Bares, T. Chapin, J. H. C. Cornelissen, M. Diemer, J. Flexas, E. Garnier, P. K. Groom, J. Gulias, K. Hikosaka, B. B. Lamont, T. Lee, W. Lee, C. Lusk, J. J. Midgley, M.-L. Navas, Ü. Niinemets, J. Oleksyn, N. Osada, H. Poorter, P. Poot, L. Prior, V. I. Pyankov, C. Roumet, S. C. Thomas, M. G. Tjoelker, E. J. Veneklaas, and R. Villar. 2004. The worldwide leaf economics spectrum. Nature 428:821–827.

Yan, Z., J. Sardans, J. Peñuelas, M. Detto, N. G. Smith, H. Wang, L. Guo, A. C. Hughes, Z. Guo, C. K. F. Lee, L. Liu, and J. Wu. 2023. Global patterns and drivers of leaf photosynthetic capacity: The relative importance of environmental factors and evolutionary history. Global Ecology and Biogeography:668–682.

Yuan, W., Y. Zheng, S. Piao, P. Ciais, D. Lombardozzi, Y. Wang, Y. Ryu, G. Chen, W. Dong, Z. Hu, A. K. Jain, C. Jiang, E. Kato, S. Li, S. Lienert, S. Liu, J. E. M. S. Nabel, Z. Qin, T. Quine, S. Sitch, W. K. Smith, F. Wang, C. Wu, Z. Xiao, and S. Yang. 2019. Increased atmospheric vapor pressure deficit reduces global vegetation growth. Science Advances 5:1–12.

Ziehn, T., J. Kattge, W. Knorr, and M. Scholze. 2011. Improving the predictability of global CO_2 assimilation rates under climate change. Geophysical Research Letters 38:L10404.

SUPPLEMENTARY MATERIAL FOR "The cost of resource use for photosynthesis drives variation in leaf nitrogen content across a climate and resource availability gradient"

Calculations for soil water holding capacity

Water holding capacity (θ_{WHC}; mm) was calculated as a function of the volumetric soil water storage at field capacity, W_{PWP} ($m^3\ m^{-3}$), and the volumetric soil water storage at wilting point:

$$\theta_{WHC} = (W_{FC} - W_{PWP})(1 - f_{gravel}) * \min\{z_{bedrock}, z_{max}\} \quad \text{(S1)}$$

where W_{FC} ($m^3\ m^{-3}$) is the volumetric soil water storage at field capacity, W_{PWP} ($m^3\ m^{-3}$) is the volumetric soil water storage at wilting point, f_{gravel} (%) is the fraction of gravel content in soil, $z_{bedrock}$ (mm) is the distance to bedrock, and z_{max} (mm) is the maximum allowable distance to bedrock, set to 2000mm. W_{FC} is calculated as:

$$W_{FC} = k_{fc} + (1.283 * (k_{fc})^2 - 0.374 * k_{fc} - 0.015 \quad \text{(S2)}$$

where

$$k_{fc} = -0.251 * f_{sand} + 0.195 * f_{clay} + 0.011 * f_{OM} + 0.006 + 0.006 * (f_{sand} * f_{OM}) - 0.027 * (f_{clay} * f_{OM}) + 0.452 * (f_{sand} * f_{clay}) + 0.299 \quad \text{(S3)}$$

W_{PWP} is calculated as:

$$W_{PWP} = k_{pwp} + (0.14 * k_{pwp} - 0.02) \quad \text{(S4)}$$

where

$$k_{pwp} = -0.024 * f_{sand} + 0.487 * f_{clay} + 0.006 * f_{OM} + 0.005 * (f_{sand} * f_{OM}) - 0.013 * (f_{clay} * f_{OM}) + 0.068 * (f_{sand} * f_{clay}) + 0.031 \quad \text{(S5)}$$

In Equations (S3) and (S5), f_{sand} (%) is the fraction of sand content in soil (%), f_{clay} (%) is the fraction of clay content in soil (%), and f_{OM} is the fraction of organic matter in soil (%). Organic matter in the soil was calculated in this study by converting soil organic carbon data extracted from SoilGrids 2.0 to soil organic matter using the van Bemmelen factor (1.724 conversion factor).

Table S1 List of sampled species, including the NRCS symbol, photosynthetic pathway, growth duration, growth habit, N fixation capability, assigned plant functional group, and the number of collected individuals

Symbol	Species	Photosynthetic pathway	Growth duration	Growth habit	N-fixer?	Plant functional group	Number sampled
ACAN11	*Acaciella angustissima* (Mill) Britton & Rose	c3	perennial	forb	yes	c3_legume	3
AMAR2	*Ambrosia artemisiifolia* L.	c3	annual	forb	no	c3_nonlegume	25
AMPS	*Ambrosia psilostachya* DC.	c3	perennial	forb	no	c3_nonlegume	32
ARAL3	*Argemone albiflora* Hornem.	c3	annual	forb	no	c3_nonlegume	3
ARPU9	*Aristida purpurea* Nutt.	c4	perennial	graminoid	no	c4_nonlegume	2
ASAS	*Asclepias asperula* (Decne.) Woodson	c3	perennial	forb	no	c3_nonlegume	3
ASLA4	*Asclepias latifolia* (Torr.) Raf.	c3	perennial	forb	no	c3_nonlegume	3
ASSY	*Asclepias syriaca* L.	c3	perennial	forb	no	c3_nonlegume	18
BOIS	*Bothriochloa ischaemum* (L.) Keng	c4	perennial	graminoid	no	c4_nonlegume	6
BOSA	*Bothriochloa saccharoides* (Sw.) Rydb.	c4	perennial	graminoid	no	c4_nonlegume	6
CAPL3	*Carex planostachys* Kunze	c4	perennial	graminoid	no	c4_nonlegume	3
CAREX	*Carex spp.* L.	c4	perennial	graminoid	no	c4_nonlegume	16
CHFE3	*Chamaesyce fendleri* (Torr. & A. Gray) Small	c3	perennial	forb	no	c3_nonlegume	2
CHPI8	*Chyrysopsis pilosa* Nutt.	c3	annual	forb	no	c3_nonlegume	3
COCO13	*Conoclinium coelestinum* (L.) DC.	c3	perennial	forb	no	c3_nonlegume	3
COER	*Commelina erecta* L.	c3	perennial	forb	no	c3_nonlegume	3
CRGLL	*Croton glandulosus* L.	c3	annual	forb	no	c3_nonlegume	22
CYDA	*Cynodon dactylon* (L.) Pers.	c4	perennial	graminoid	no	c4_nonlegume	15
DIAN	*Dichanthium annulatum* (Forssk.) Stapf	c4	perennial	graminoid	no	c4_nonlegume	8
ENPE4	*Engelmannia peristenia* (Raf.) Goodman & C.A. Lawson	c3	perennial	forb	no	c3_nonlegume	6
EUMA8	*Euphorbia marginata* Pursh	c3	annual	forb	no	c3_nonlegume	6
GAPU	*Gaillardia pulchella* Foug.	c3	annual	forb	no	c3_nonlegume	16
GLGO	*Glandularia gooddingii* (Briq.) Solbrig	c3	perennial	forb	no	c3_nonlegume	2

Symbol	Species	Photosynthetic pathway	Growth duration	Growth habit	N-fixer?	Plant functional group	Number sampled
HEAN3	*Helianthus annuus* L.	c3	annual	forb	no	c3_nonlegume	6
HECA8	*Heterotheca canescens* (DC.) Shinners	c3	perennial	forb	no	c3_nonlegume	2
HETE3	*Heliotropium tenellum* (Nutt.) Torr	c3	annual	forb	no	c3_nonlegume	3
IVAX	*Iva axillaris* Pursh	c3	perennial	forb	no	c3_nonlegume	4
LIAT	*Lilaeopsis attenuata* auct. non (Hook. & Arn.) Fernald	c3	perennial	forb	no	c3_nonlegume	3
LIPU	*Liatris punctata* Hook.	c3	perennial	forb	no	c3_nonlegume	3
LOPE	*Lolium perenne* L.	c3	perennial	graminoid	no	c3_nonlegume	9
MIQU2	*Mimosa quadrivalvis* L.	c3	perennial	forb	yes	c3_legume	15
NALE3	*Nassella leucotricha* (Trin. & Rupr.) Pohl	c3	perennial	graminoid	no	c3_nonlegume	19
OECU2	*Oenothera curtiflora* W.L. Wagner & Hoch	c3	annual	forb	no	c3_nonlegume	3
OENOT	*Oenothera spp.* L.	c3	annual	forb	no	c3_nonlegume	1
PAVI2	*Panicum virgatum* L.	c4	perennial	graminoid	no	c4_nonlegume	12
RACO3	*Ratibida columnifera* (Nutt) Wooton & Standl.	c3	perennial	forb	no	c3_nonlegume	40
RHSET	*Rhynchosia senna* Gillies ex Hook. var. *texana* (Torr. & A. Gray) M.C. Johnst.	c3	perennial	forb	yes	c3_legume	1
RUHI2	*Rudbeckia hirta* L.	c3	perennial	forb	no	c3_nonlegume	3
RUNU	*Ruellia nudiflora* (Engelm. & A. Gray) Urb.	c3	perennial	forb	no	c3_nonlegume	15
RUTR	*Rubus trivialis* Michx.	c3	perennial	vine	no	c3_nonlegume	3
SAFA2	*Salvia farinacea* Benth.	c3	perennial	forb	no	c3_nonlegume	7
SCHIZ4	*Schizachyrium spp.* Nees	c4	perennial	graminoid	no	c4_nonlegume	8
SCSC	*Schizachyrium scoparium* (Michx.) Nash	c4	perennial	graminoid	no	c4_nonlegume	3
SODI	*Solanum dimidiatum* Raf.	c3	perennial	forb	no	c3_nonlegume	1
SOEL	*Solanum elaeagnifolium* Cav.	c3	perennial	forb	no	c3_nonlegume	53
SOHA	*Sorghum halapense* (L.) Pers.	c4	perennial	graminoid	no	c4_nonlegume	38
STTE3	*Stillingia texana* I.M. Johnst.	c3	perennial	forb	no	c3_nonlegume	3
VEOC	*Verbesina occidentalis* (L.) Walter	c3	perennial	forb	no	c3_nonlegume	3
VEST	*Verbena stricta* Vent.	c3	perennial	forb	no	c3_nonlegume	3

Table S2 Model selection results for soil moisture, air temperature, and vapor pressure deficit. Soil moisture was used in a bivariate regression against β, while vapor pressure deficit (*VPD*) was used in bivariate regressions against leaf C_i:C_a*

	Soil moisture		***VPD***	
Day	AICc	RMSE	AICc	RMSE
1	3067.01	4.7320	-890.77	0.0731
2	3066.78	4.7308	-890.39	0.0731
3	3066.72	4.7304	-890.27	0.0731
4	3066.80	4.7310	-889.77	0.0731
5	3066.96	4.7319	-889.73	0.0731
6	3067.02	4.7323	-889.66	0.0731
7	3067.11	4.7327	-889.62	0.0731
8	3067.16	4.7331	-889.52	0.0731
9	3067.23	4.7336	-889.60	0.0731
10	3067.34	4.7343	-890.38	0.0730
15	3067.39	4.7356	-889.97	0.0731
20	3067.20	4.7355	-890.11	0.0731
30	3066.97	4.7343	-890.99	0.0731
60	3063.82	4.7195	-890.97	0.0731
90	**3058.92**	**4.6964**	**-906.72**	**0.0720**

*Timescale that conferred lowest AICc value is indicated in bold.

Figure S1

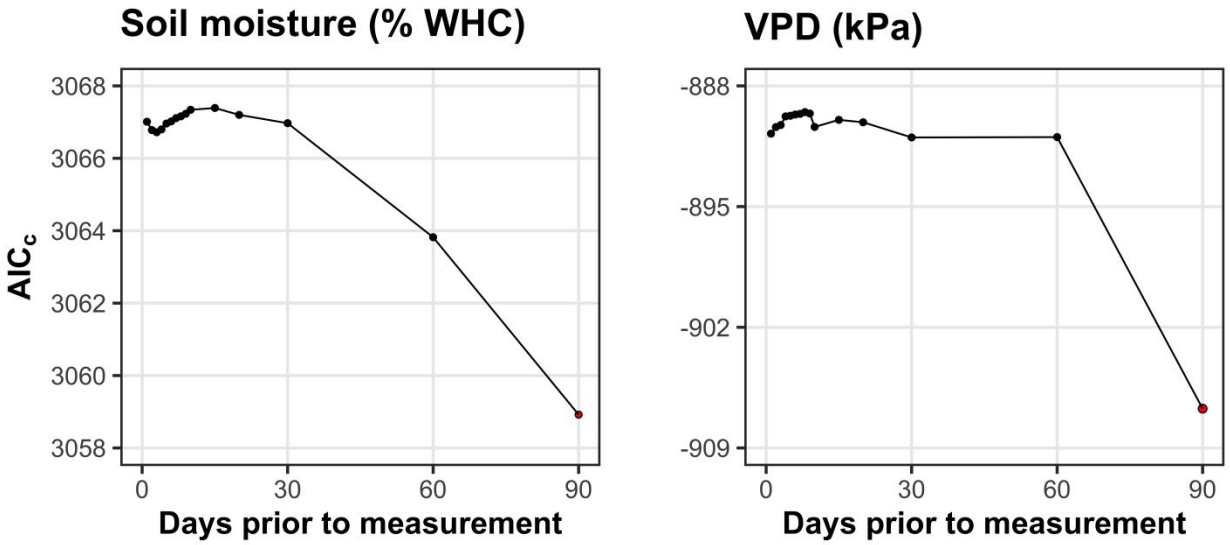

Fig. S1 Model selection results exploring relevant timescales for soil moisture (left panel) and vapor pressure deficit (right panel). The x-axis indicates the number of days before each site visit and the y-axis notes the corrected Akaike Information Criterion value. The timescale with the lowest AICc value, and therefore most relevant timescale to include in statistical models, is noted as a red point.

Figure S2

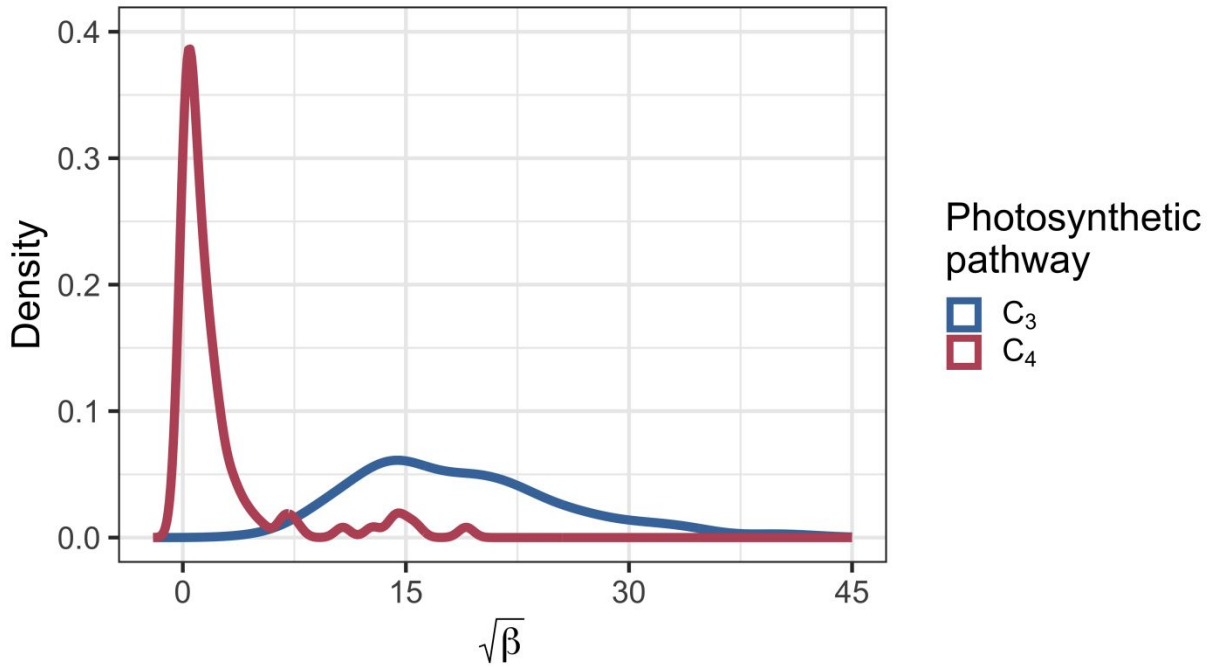

Fig. S2 Density plot demonstrating the observed variance in β across the environmental gradient. Square root transformed β is included on the x-axis. Blue shading indicates the distribution of β values for C_3 species, while red shading indicates the distribution of β values for C_4 species.